

PARAGENESIS OF COBALT AND NICKEL AT THE BLACK BUTTE
COPPER PROJECT, MEAGHER COUNTY, MONTANA

by
Joshua White

A thesis submitted in partial fulfillment of the
requirements for the degree of

Master of Science in Geosciences
Geology Option

Montana Tech of The University of Montana
2012

Abstract

The Black Butte Copper Project (formerly known as the Sheep Creek deposit) is a sediment hosted, laterally extensive massive sulfide deposit hosted in the mid-Proterozoic Newland Formation in Central Montana. Formation of the deposit occurred during two stages of mineralization: Stage I occurred during deposition of sediment in the Helena Embayment, and Stage II occurred post-deposition. Stage I mineralization is characterized by a large quantity of porous pyrite hosting significant Co/Ni/As mineralization in the form of both ion substitution within the pyrite chemical lattice and small ($< 1 \mu\text{m}$) mineral inclusions of Ni-rich alloclasite. Stage II mineralization reworked the existing Co/Ni/As mineralization, removing the metals from the pyrite and reprecipitating them as distinct siegenite $((\text{Co,Ni})_3\text{S}_4)$ and tennantite $(\text{Cu}_{12}\text{As}_4\text{S}_{13})$ grains, usually adjacent to one another. Stage II introduced minor, if any, additional Co/Ni/As mineralization into the deposit. Although siegenite is abundant in Co-rich portions of the ore body and is readily identifiable in hand specimen and under the microscope, stoichiometric relationships based on drill-core assay data suggest that Co and Ni were originally introduced into the deposit in the form of alloclasite.

Although many of the characteristics of SEDEX type deposits are present at Black Butte (e.g., low temperature of formation, laterally extensive massive sulfide horizons, interbedded black shales, abundant barite and local phosphate horizons, hosted within a continental rift) the lack of economic Pb and Zn mineralization in the central ore body and the abundance of Cu/Co/Ni is more typical of red-bed copper deposits. The Neihart Quartzite, resting below the base of the Belt Supergroup, is a possible source bed for Cu-rich ore fluids, which, depending on the pH and redox state, may have been rich in Co and Ni as well.

Keywords: Paragenesis, Sheep Creek, SEDEX, Belt Supergroup, Cobalt, Hydrothermal

Dedication

I would like to make three dedications for all of my work with this thesis. Without these three I would not be the person I am today, nor would I be where I am today. First, I wish to dedicate this thesis to my Lord and Savior, Jesus Christ. Frequently religion, and specifically the Christian religion, is discounted within the scientific community as a compilation of myths relied upon by primitive peoples before they devised the scientific method to properly explain their world. I would like to acknowledge their point of view, but state that scientists are fallible just like everyone else. I met Jesus a long time ago, but 7 years ago while I was serving with the Marine Corps in Iraq, he saved my life, quite literally, and because of that I can withstand as many scoffers as care to find me.

Second, I dedicate this thesis to the two most important people in my life: my wife Elizabeth and my daughter Ava. I am very fortunate to have them both and I am so glad that they were able to share the last two years here at Montana Tech with me. Girls, I love you.

Acknowledgements

I wish to thank Tintina Resources for their generous financial support of this research project as well as all of the information that they provided to assist with my research. Jerry Zieg, the Vice President of Exploration at Tintina, is deserving of special recognition. He was the person who approved funding for the project, and also pointed out a variety of needed corrections near the end of project. Without his revisions this thesis would have had some glaring inaccuracies concerning the geologic setting and exploration history. Also, I wish to thank Gary Wyss and the Center for Advanced Mineral and Metallurgical Processing for all of his time and effort with the Scanning Electron Microscope that were so valuable to this investigation. Also, thanks are in order for Professor Michael Rowe at Washington State University for lending us his time and instruction with the Electron Microprobe (without which we never would have identified allosclerite!). Thanks to both Dick Berg of the Montana Bureau of Mines and Geology and Diane Wolfgram of Montana Tech for their reviews and revisions, as well as for acting as committee members for the review of this thesis.

Finally, and by far most importantly, I would like to thank Dr. Chris Gammons, my advisor. He envisioned this project and suggested that I work on it. In fact, initially, I was interested in the hydrogeology of mining, but he suggested that studying ore mineralogy may be a better way to ensure a successful career in mining. And after starting this project, I have never looked back. This project has enthralled me and I am indeed looking forward to a career as a mine geologist. Throughout the course of this project, both with respect to the writing and the research, his input and advice have been too valuable to put a price on. Without him this thesis would not exist, and I would not be looking forward to my new position as a mine geologist. Chris, honestly, I can't thank you enough.

Table of contents

ABSTRACT	II
DEDICATION	III
ACKNOWLEDGEMENTS	IV
LIST OF TABLES	VII
LIST OF FIGURES.....	VIII
LIST OF PLATES.....	IX
1. INTRODUCTION	1
1.1. Purpose and Scope of the Project.....	1
1.2. Description of Black Butte	2
2. METHODS	13
2.1. Sample Collection.....	13
2.2. Optical Petrography.....	14
2.3. SEM and Electron Microprobe Analysis.....	15
2.4. Stable Isotopes of Carbonate Minerals	16
2.5. Assay Data	16
3. RESULTS.....	17
3.1. Core Samples.....	17
3.2. Microscopy and SEM.....	19
3.3. Assay Data	45
3.4. Carbon Isotopes	51
4. DISCUSSION.....	54
4.1. Mineralization at Black Butte.....	54
4.2. Physical and chemical conditions of ore formation.....	58
4.3. Source of metals.....	63

4.4.	<i>Comparison of Black Butte to other ore-deposit models</i>	65
5.	CONCLUSIONS AND RECOMMENDATIONS	70
5.1.	<i>Conclusions</i>	70
5.2.	<i>Possible future work</i>	72
6.	REFERENCES	74
	APPENDIX A: PHOTOMICROGRAPH LOCATIONS	79
	APPENDIX B: EDS ANALYSES	80

List of Tables

Table 1: Indicated and Inferred Resources Courtesy of Tintina Resources	12
Table 2: Pyrite Types.....	20
Table 3: EMPA Analyses of Pyrite Grains	22
Table 4: EMPA analyses of Chalcopyrite Grains	28
Table 5: EMPA Analyses of Tennantite Grains.....	28
Table 6: EMPA Analyses of Siegenite Grains	33
Table 7: EMPA Analyses of Alloclasite Grains.....	34
Table 8: EMPA Analyses of Galena, Sphalerite, and Bismuthinite Grains	41
Table 9: Carbonate Isotope Results	52

List of Figures

Figure 1: Location of Black Butte (Courtesy of Tintina Resources)	2
Figure 2: Belt-Purcell Basin (Modified from Lydon, 2007)	3
Figure 3: Surface Map of Black Butte (Courtesy of Tintina Resources)	9
Figure 4: Cross-section of the Johnny Lee Deposit (Courtesy of Tintina Resources) .	9
Figure 5: Core Holes Sampled	14
Figure 6: Photographs of Drill Core	18
Figure 7: Black Butte Siegenite Analyses	32
Figure 8: Composition of Feldspars from Black Butte	44
Figure 9: Pyrite and Chalcopyrite Plots	45
Figure 10: Cobalt Assay Relationships	47
Figure 11: Silver Mineralization Plots	49
Figure 12: Phosphorous Plots	50
Figure 13: Isotopic Composition of Carbonate as a Function of Depth	53
Figure 14: Paragenesis Diagram	55
Figure 15: Crystal structure comparison of marcasite, glaucodot, and alloclasite ...	58
Figure 16: aS₂-Temperature Diagram for Minerals Found at Black Butte	62
Figure 17: Adsorption of Cu, Pb, Zn, Co, and Ni onto Goethite as a Function of pH	65

List of Plates

Plate 1: Pyrite Types	23
Plate 2: Other Iron Sulfides	24
Plate 3: Pyrite “Vent Fauna”	26
Plate 4: Copper Mineralization	29
Plate 5: LSZ Cobalt Minerals I	35
Plate 6: LSZ Cobalt II	36
Plate 7: USZ Cobalt I	38
Plate 8: USZ Cobalt II	39
Plate 9: Lead and Zinc Mineralization	42

1. Introduction

1.1. Purpose and Scope of the Project

The Black Butte copper (+ cobalt, silver) deposit, formerly known as the Sheep Creek deposit, is located approximately 20 miles northwest of White Sulphur Springs in central Montana (Figure 1). It is a laterally extensive massive sulfide deposit comprised of several distinct ore bearing sulfide horizons. Black Butte has three primary economic metals: copper, cobalt, and silver. Copper, the primary economic metal, has been extensively studied and there are already several articles by previous workers that discuss the copper mineralization (Zieg et al., 1991; Himes & Petersen, 1990; Graham et al., 2012). However, cobalt, along with silver, has the potential to substantially improve economic returns at Black Butte. Other than some reconnaissance work by Himes & Petersen (1990), very little is known about the mineral setting of Co, Ni and Ag at Black Butte. With an average historical price of \$5.79 a pound (2009 USD), and a current price of \$13.83 (April 18, 2012, www.infomine.com), cobalt has the potential to substantially increase the profitability of the deposit, provided it is economically recoverable. The question of cobalt recovery is one of metallurgy; whether or not it would be economic to design the mill to recover the cobalt in addition to the copper. Therefore, a better understanding of the mineralogy of Co and Ni at Black Butte was a major objective of this project.

This chapter is an introduction to the Black Butte deposit, and includes an overview of the regional and local geologic setting, followed by a summary of current and past exploration.

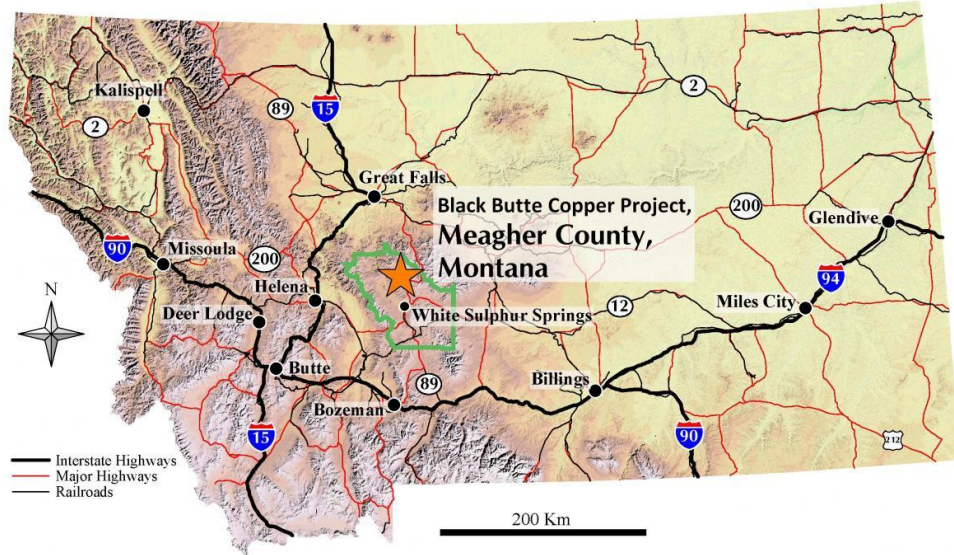


Figure 1: Location of Black Butte (Courtesy of Tintina Resources)

1.2. Description of Black Butte

1.2.1. Regional Geology

The Belt-Purcell Basin covers an area of approximately 200,000 km² extending from southern British Columbia (B.C.), Canada, into the northern United States (Chandler, 2000) and is filled with a Mesoproterozoic SuperGroup of sedimentary rocks. The basin hosts a variety of different ore bodies (e.g., see Lydon, 2007) including the giant Sullivan Pb-Zn-Ag Mine, in B.C., the world class, vein-type Ag-Pb-Zn deposits of the Coeur d'Alene District, Idaho, the Spar Lake, Rock Creek, and Montanore disseminated Cu-Ag deposits in NW Montana, and the Black Butte deposit of this study (Figure 2).

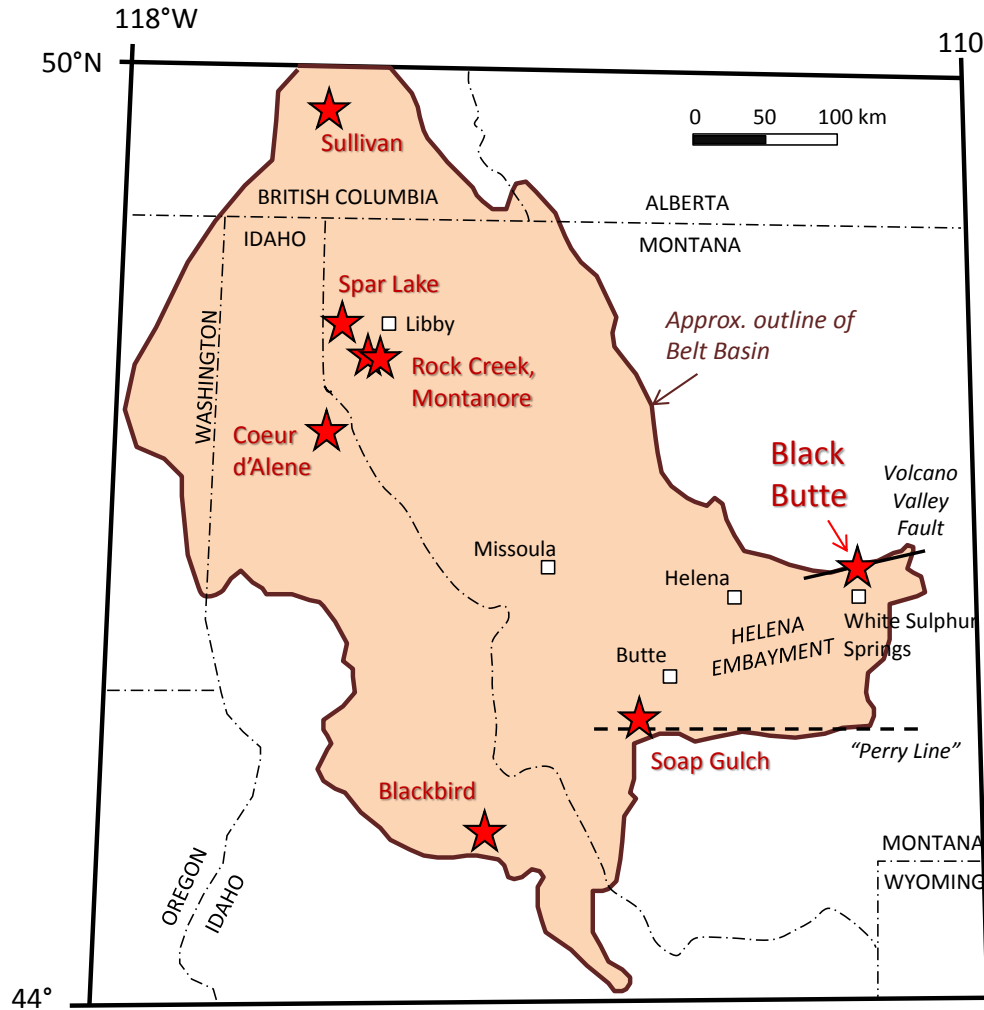


Figure 2: Belt-Purcell Basin (Modified from Lydon, 2007)

The Belt basin formed approximately 1.5Ga ago as an intracontinental rift and is comprised of a main branch and an eastern limb (Winston, 1986a; Chandler, 2000; Sears, 2007; and references therein). The main basin is approximately 750 km long, trends to the north-northwest, and contains the Sullivan and Spar Lake mines. The eastern limb, known as the Helena Embayment, contains the Black Butte ore body. The sediment which fills the southern portion of the basin is divided into four main stratigraphic divisions. These are, from the bottom up, the Lower Belt sequence, the Ravalli Group, the Middle Belt Carbonate, and the Missoula

Group (Winston, 1986b; Chandler, 2000). The Lower Belt sequence of the main branch of the basin contains a 12 km thick turbidite complex known as the Aldridge Fm. in Canada and the Prichard Fm. in the U.S. (Lydon, 2007). Mafic sills, collectively, may comprise up to 40% of the Aldridge Fm. in Canada (Höy et al., 2000), and are present to a lesser extent in the Prichard Formation.

The Helena Embayment is asymmetric and trends east-west. The southern margin, sometimes referred to as the “Perry Line”, is comprised of LaHood Conglomerate submarine fans and debris flows. The LaHood Fm. hosts the much younger Golden Sunlight epithermal gold mine near Whitehall, MT. In the northern Embayment the LaHood grades into finer grained sedimentary rocks of the Chamberlain, Newland and Greyson Fms. (Graham et al., 2012, and references therein). Near the northern margin of the Helena Embayment, where Black Butte is located, the LaHood has given way completely to the Chamberlain and Newland Formations, which are overlain by the Greyson Formation (McMannis, 1963).

In the main basin above the Lower Belt lies the Ravalli Group that is comprised of shallow water sediments and is thought to represent a major regression event (Connor et al., 1984). The Middle Belt Carbonate is a carbonate rich sequence of marine sediments believed to be a transgression event (Grotzinger, 1986). Finally, the Missoula Group is mostly sand rich alluvium which grades into shallow marine sediments to the east and north (Chandler, 2000). In the Helena Embayment neither the upper half of the Middle Carbonate nor the Missoula Group are present (Graham et al., 2012).

There has been much debate about the formation of the Belt Basin. Whether the subaqueous depositional environment was lacustrine or marine is not known (Chandler, 2000), nor is it known if the deeper water column was oxidized or anoxic (Goodfellow, 2000).

Likewise, there have been several models proposed to explain the tectonic setting of the basin. Some proposed models (summarized by Graham et al., 2012) include a rift basin (Höy et al., 2000 and references therein), an intracratonic lake (Winston, 1986a), a continental-margin delta (Price, 1964), and a back-arc basin formed during convergence along western North America (Ross and Villeneuve, 2003).

The main branch of the Belt Basin has been subjected to at least three episodes of deformation (Price and Sears, 2000). These include an episode of left lateral transpression during the Late Jurassic-Early Cretaceous followed by a right lateral transpression during the Late Cretaceous-Paleocene as part of the Laramide Orogeny, both of which resulted in compression. Finally, there was an early Tertiary episode of crustal extension (Price and Sears, 2000). Of these three events only the Late Cretaceous-Paleocene transpression event affected the Helena Embayment (Graham et al., 2012).

The Helena Embayment varies geologically from the main branch of the Belt Basin in a variety of ways, including apparently less metamorphism (Maxwell and Hower, 1967), and an absence of the upper most stratigraphy seen in the main basin (i.e. the upper Middle Belt carbonate and the Missoula Group). The sediment in the Helena Embayment is metamorphosed to lower greenschist facies, and primary sedimentary textures are well-preserved, as seen in the Neihart Quartzite and the LaHood Fm. which consists primarily of siltite and argillite (mildly metamorphosed fine grained clastic sedimentary rocks). McMannis (1963) suggests that the detrital source may have been completely eroded away by the time the uppermost stratigraphy of the Helena Embayment (the upper Greyson Fm.) was being deposited, as evidenced by the decrease in arkose content with decreasing depth. McMannis (1963) also shows that there was

variation in the depositional environment within the Helena Embayment, as the arkose content decreases laterally to the north.

1.2.2. Local Geology

1.2.2.1. Stratigraphy

Black Butte is hosted within the Lower Belt stratigraphy of the Helena Embayment. Basement rocks in the Helena Embayment are comprised of granitic gneiss unconformably overlain by the Proterozoic Neihart Quartzite. The Neihart is a pink quartzite that is laterally extensive, forming a sheet like layer of metasediment on top of the basement erosional surface. Schieber (1989) suggested that the Neihart, a texturally mature quartzite, was deposited before the opening of the Belt Basin by braided stream and shoreline environments. The Neihart Fm. is approximately 270m thick in the vicinity of Black Butte, as reported by Keefer (1972) and confirmed with drill core by Tintina Resources during the ongoing drilling program.

Above the Neihart lies the Chamberlain Fm., a near-shore mudflat deposit (Godlewski and Zieg, 1984), which has been shown to be approximately 200m thick in the vicinity of Black Butte during the ongoing Tintina drilling program (G.A. Zieg, personal communication, April 3, 2012). This unit is primarily black micaceous shale with uneven laminations. The Lower Chamberlain contains abundant sand lenses, whereas the Upper Chamberlain is dominated by lenses of dolomite (Godlewski and Zieg, 1984).

Directly above the Chamberlain lies the Newland Formation which contains the Black Butte orebody. The Newland was divided by Nelson (1963) into a lower member being mainly dolomitic shale, and an upper member being mainly dolomite with some shale layers. Between the two members are beds of feldspathic sandstone which have been labeled the 'Newland Transition Zone' (Schieber, 1985). The Newland Fm. ranges in thickness from 600 m to 3000 m,

with a general thickening to the south (Chandler, 2000). At the Black Butte ore body the Newland has a total thickness of approximately 1100 m based upon drilling and measured sections done by Zieg (1986). In the Johnny Lee area of the deposit, the Lower Newland contains abundant debris flows, possibly filling in paleochannels or aprons shed from fault scarps (Graham et al., 2012). The Lower Newland in the Lowry area of the Black Butte deposit contains brecciated shale and minor debris flows (Graham et al., 2012). Conversely, the Upper Newland is defined by alternating shale and carbonate units with very minor interbedded sandstones. Fluid inclusion data from barite found in the upper part of the Black Butte ore deposit suggest a water depth of at least 850 m during mineralization (Himes and Petersen, 1990).

Most of the presently-defined, copper-rich sulfide horizons at Black Butte are contained within the Lower Newland Fm. Sulfide mineralization was not limited to the Lower Newland, however, as there are two smaller copper-rich and multiple pyrite-rich sulfide horizons in the Upper Newland (G.A. Zieg, pers. communication, April, 2012).

1.2.2.2. Structure

The Volcano Valley Fault dominates the structure at Black Butte, and its location approximates that of the Proterozoic “buttress fault” (G.A. Zieg, pers. communication, April, 2012). The Helena Embayment opened during middle Proterozoic time, as an asymmetric graben type structure with modest normal faults forming its northern margin and much larger normal faults along its southern margin (McMannis, 1963; Sears, 2007). The buttress fault(s) at Black Butte formed the northern margin of most of the Newland Formation in the Helena Embayment in that area, an interpretation supported by a concentration of debris flow conglomerate within the Newland Formation along the trace of the buttress fault. Zieg (personal communication,

2012) believes the northern embayment margin formed as a series of fault blocks dropped at progressively deeper elevations, in stairstep fashion, from north to south.

The Volcano Valley Fault developed as a reverse fault during Laramide time with a component of left lateral strike slip movement (Woodward, 1983; Sears, 2007). At Black Butte, this fault moved Newland shale and carbonate up the middle Proterozoic series of fault blocks which form the northern margin of the embayment, and placed it adjacent to the basal Neihart Quartzite (labeled “quartzite” in Figure 4), a northward-thinning section of Chamberlain and lowermost Newland Fm., as well as the overlying Cambrian-aged Flathead Sandstone (labeled “sandstone” in Figure 4). The Volcano Valley fault bends at Black Butte from ENE to ESE and the highly-mineralized Johnny Lee zone is located in the hanging wall at the bend of the fault (Figures 3 and 4).

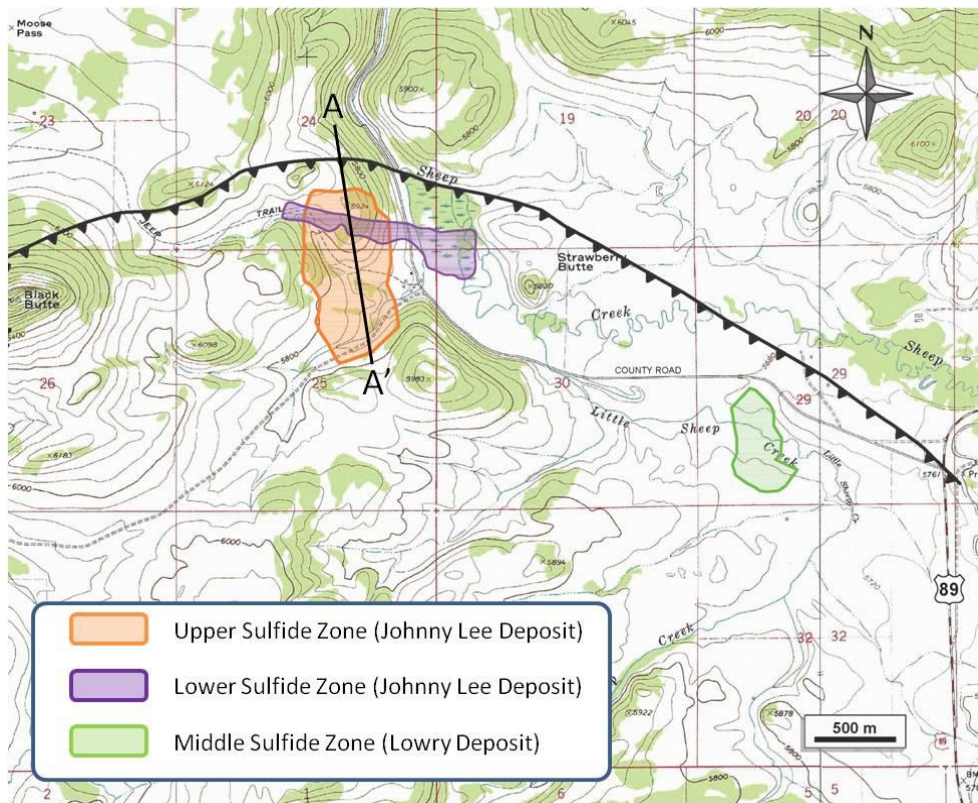


Figure 3: Surface Map of Black Butte (Courtesy of Tintina Resources)
See Figure 4 for cross-section along A-A'.

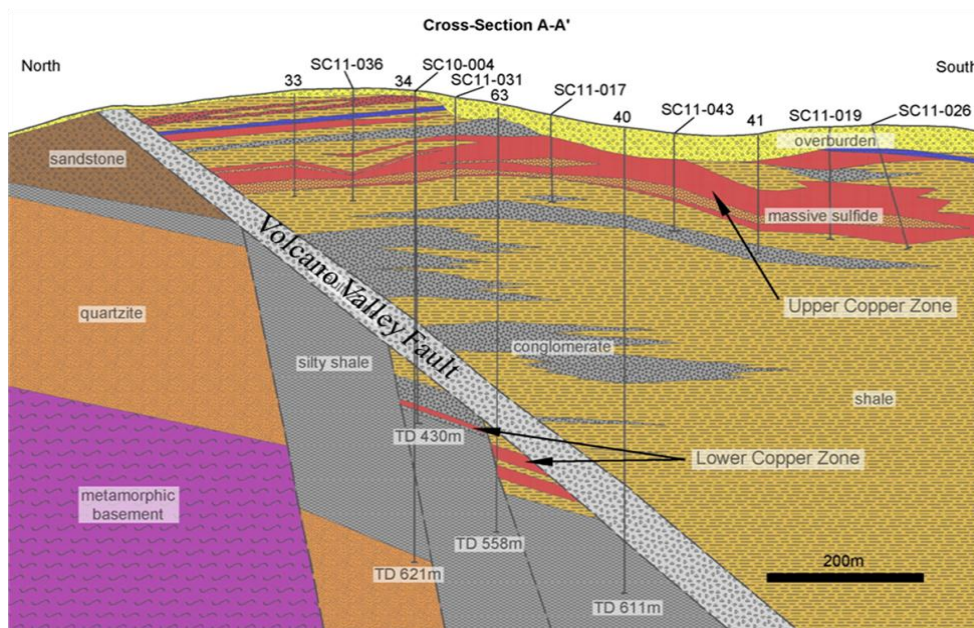


Figure 4: Cross-section of the Johnny Lee Deposit (Courtesy of Tintina Resources)
The unit labeled "quartzite" is the Neihart Fm.

1.2.2.1. Mineralization

The Black Butte ore body is defined by laterally extensive, shale-hosted, massive-pyrite horizons. Black Butte contains at least 10 mineralized sulfide horizons, five of which contain copper (G.A. Zieg, pers. communication, April, 2012). Three of these copper-bearing sulfide horizons are of greatest interest to the company at the time of writing, and are referred to as the Lower, Middle, and Upper Sulfide Zones (LSZ, MSZ, and USZ, respectively). The USZ and LSZ are the dominant mineralized zones in the Johnny Lee Deposit, and the MSZ is more important in the Lowry Deposit. Only the USZ from the Johnny Lee and LSZ from both the Johnny Lee and Lowry (Figure 3) were examined in this thesis, due to the abundance of available drill core at the time of sampling for those two locales.

On a district scale there are significant levels of Pb and Zn within the Newland Fm., but none identified as being large enough to mine at the present time. The southern and western portions of the district are enriched in Pb and Zn, while the northern and central portions are more enriched in Cu and Co (G.A. Zieg, pers. communication, April 2012). Because the larger accumulation of mineralization is the Cu-Co-rich central portion, the deposit is referred to as a Cu-Co deposit, rather than a Pb-Zn deposit. Jerry Zieg suggests that the Pb-Zn mineralization was separated in both space and time from the Cu-Co mineralization, an idea which is strengthened by the findings of this study as discussed in chapter 4.

In addition to pyrite, both the USZ and LSZ contain high concentrations of chalcopyrite, the main Cu-sulfide ore mineral, as well as lesser amounts of marcasite, tennantite, sphalerite, and galena (Himes and Petersen, 1990; Graham et al., 2012). The ongoing drilling project has also identified local enrichments in bornite scattered throughout the deposit. Both the USZ and LSZ are highly enriched in cobalt, nickel, and silver (Himes and Petersen, 1990), although the

mineral form of these three metals is poorly understood, and nickel is not recognized as contributing economically to the deposit at the time of writing. In addition, the LSZ is locally enriched in gold.

The gangue mineralogy of the LSZ is dominated by dolomite and quartz. The USZ is rich in quartz and barite, with relatively less dolomite. Graham et al. (2012) interpret the lack of dolomite in the USZ to indicate that silicification was widespread during USZ mineralization. Both the USZ and the LSZ also contain localized accumulations of apatite.

1.2.3. Exploration History

Black Butte was discovered in the early 20th century by the extensive gossan outcrops that developed on top of the massive sulfide by natural weathering (Himes and Petersen, 1990). There were at least two mining operations in the vicinity of Black Butte during this period, including the Virginia mine near the present day Johnny Lee area in the 1890's (Weed, 1900), and a shaft sunk by Johnny Lee, who homesteaded on the property in 1910 (Meagher County records). He didn't encounter sulfide; his shaft was approximately 500 meters west of the aptly named Johnny Lee deposit (G.A. Zieg, personal communication, April, 2012). After this, the property laid dormant until 1974, when Homestake drilled one hole into a laminated pyrite bed. Later, both Cominco and Anaconda drilled holes into sulfide beds. The economic potential for the area was realized when rich copper ore was discovered by a joint venture between Cominco American and Utah International Incorporated in the 1980's. Cominco, in a joint venture with BHP, consolidated all of the claims on the property and drilled it extensively. Due to low commodities prices at the time, however, it was deemed uneconomic to mine and was left dormant again.

In 2008, Tintina Resources acquired the property and began to drill and reprove the Johnny Lee and Lowry ore bodies. The indicated and inferred resources at the time of writing of this thesis, with respect to today's NI 43-101 standards, are shown below in Table 1.

Table 1: Indicated and Inferred Resources Courtesy of Tintina Resources

Deposit	Zone	Category	Tonnes (* 10 ⁶)	Cu grade (%)	Cu (lbs * 10 ⁶)	Co grade (%)	Co (lbs * 10 ⁶)	Ag Grade (g/t)	Ag (oz * 10 ⁶)
Johnny Lee	upper	indicated	8.83	2.96	553	0.12	22	16.9	4.61
Total		indicated	8.83	2.96	553	0.12	22	16.9	4.61
Johnny Lee	upper	inferred	1.26	2.64	73	0.1	3	16.4	0.7
Johnny Lee	Lower	inferred	2.46	4.71	256	.06	3	5.1	0.4
Lowry	Middle	inferred	5.14	2.6	294	0.12	14	14.6	2.4
Total		inferred	8.86	3.19	623	0.1	20	12.2	3.48

2. Methods

2.1. Sample Collection

Core samples were collected at the Tintina core shed in White Sulphur Springs, Montana, after having been logged by company geologists. All samples were cut from the center of the drill core with a wet saw. Samples were chosen based upon favorable metal content from assay data as well as having promising visual characteristics. Some of the more interesting minerals, such as siegenite and tennantite, appear gray under a hand lens and can be clearly seen if the crystals are large enough. During the drilling performed by Tintina Resources in 2011, company geologists identified coarse grained euhedral cobalt grains in the core that had not been previously noted and the author was asked to identify which cobalt species this was (siegenite).

Once the core samples had been collected and photographed, they were brought back to the rock laboratory in the basement of the Mining and Geology building at Montana Tech. A wet saw was used to cut pieces less than 1 inch in diameter that would be mounted in epoxy and polished. The epoxy used was transparent 2lb EPO-TEK manufactured by Epoxy Technology. Epoxy mounts were polished using a Buehler AutoMet 250, and were polished down to 0.5 microns. All polished samples were labeled with drill hole and depth information on plain white paper that was impregnated into the epoxy mount. When the information was available, an arrow indicating the 'up' direction was included as well for identification of certain textures, such as graded bedding.

Samples were collected from a wide selection of drill holes (Figure 5) representing all three sulfide zones in both the Johnny Lee and Lowry areas. However, due to preferential drilling of the USZ in Johnny Lee, the majority of samples are from there. In addition, although both ore horizons are found in the Lowry and Johnny Lee areas, Johnny Lee has been more

extensively analyzed in this study due to the abundance of drill core data. In all, 62 individual core samples were taken from 13 holes drilled during the 2010-2011 exploration program by Tintina Resources at Black Butte. For the ore microscopy and petrographic analyses, 72 polished epoxy mounts and 10 polished thin sections were prepared from these core samples.

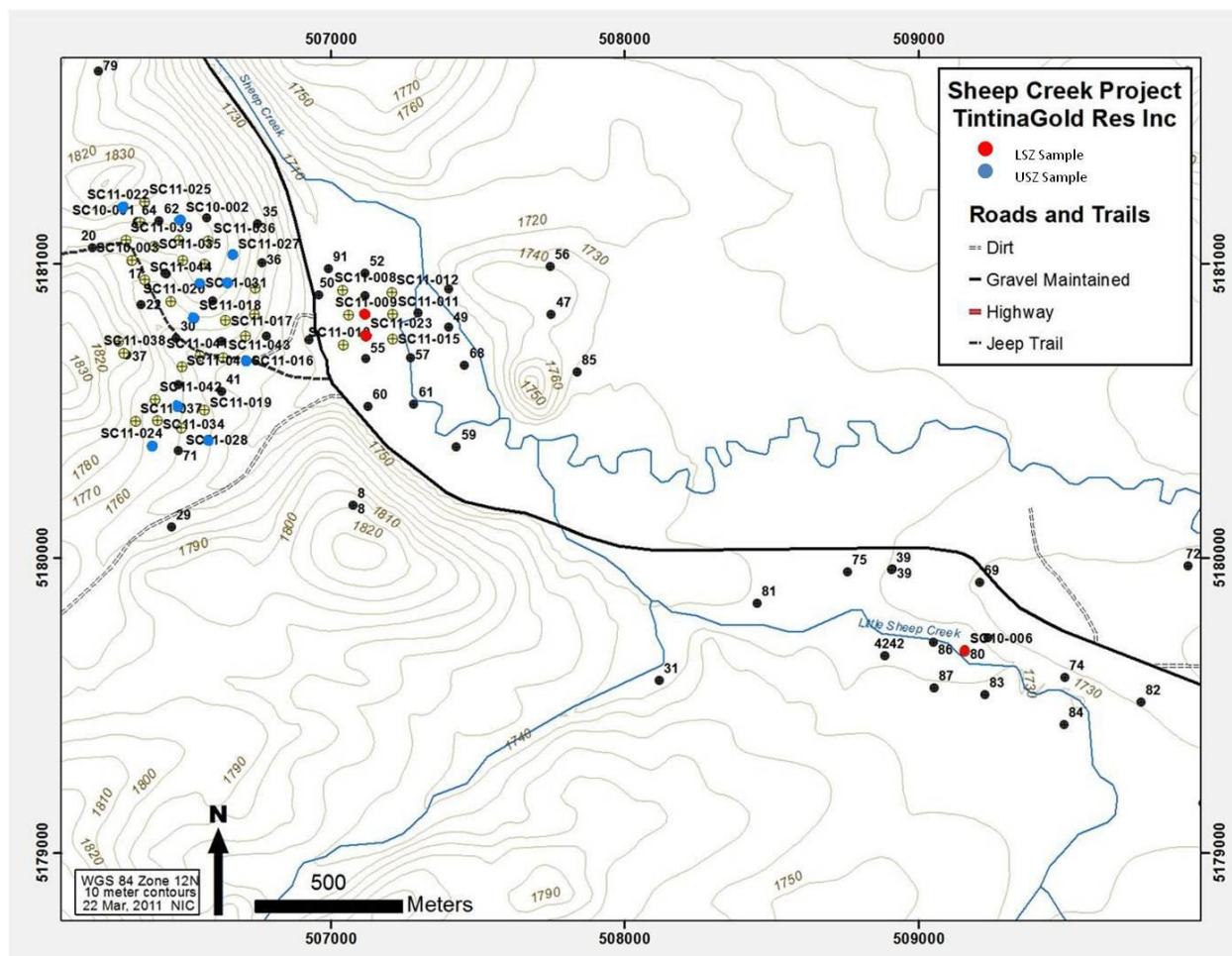


Figure 5: Core Holes Sampled

2.2. Optical Petrography

All of the polished specimens were examined under an optical microscope using reflected light (epoxy mounts) or both reflected and transmitted light (polished thin sections). An initial

identification of the important ore and gangue minerals was based on optical properties. The microscope used was an Aus Jena with four different focusing lenses: 2.5x, 10x, 20x, and 50x.

2.3. SEM and Electron Microprobe Analysis

A Scanning Electron Microscope (SEM) located in the Center for Advanced Mineral and Metallurgical Processing (CAMP) at Montana Tech was used to identify minerals found within the ore horizons at Black Butte by means of energy dispersive X-ray analysis (EDX). The machine used was a LEO 1430VP SEM, operated by Gary Wyss. Operating conditions included an acceleration voltage of 25 kV, a working distance of 18mm, a spot size of 550 nm², a probe current of 5nA, and a tungsten filament. Specimens were scanned manually, and images were generated using the backscatter electron (BSE) detector. EDX spectra, collected with an EDAX Apollo 40 detector using a 3.3 window type, a collection rate of 35,000 – 55,000 counts per second (cps), 25-30% dead time, and a collection time of 10-20 seconds, provided elemental data on each phase being identified. The EDX analyses are based upon a standardless calibration that uses a ZAF correction factor for the elements identified in the spectra acquired with the thin film silicon drift detector (SDD). The ZAF is a theoretical correction which accounts for the atomic number effect, absorption effect, and fluorescence effect.

To verify the findings of the SEM at Montana Tech, selected samples were analyzed using an electron microprobe located in the Geology Department at Washington State University in Pullman, Washington. The analyses were performed with a JEOL 8500F Field Emission Electron Microprobe (FE-EMPA), with the assistance of Dr. Michael Rowe. EMPA analyses were collected at 15kV accelerating voltage, 30 nA beam current, and a 1 µm beam size, and were standardized (WDS) for the following suite of elements: Ag, As, Au, Bi, Co, Cu, Fe, Ni,

Pb, S, Sb, and Zn. Cobaltite was used as a secondary standard for Co and Ni. Additional semi-quantitative analyses were collected by operating the EMPA in EDX mode.

2.4. Stable Isotopes of Carbonate Minerals

A representative vertical transect of sediment samples from the Newland Fm. above, within, and below the USZ was taken from drillhole SC11-021 in an effort to determine if there was any C-isotope pattern denoting where the ore horizon was located. This was done by collecting samples using a wet saw from the Tintina core shed. Once the samples were collected they were crushed in the Dept. of Metallurgical Engineering at Montana Tech using both a coarse jaw-crusher and a fine roll crusher. The crushers were cleaned using compressed air between each sample. Final preparation was done using a 100 micron sieve to collect just the finest of crushed particles. The sieved fractions were transferred into labeled glass vials and sent to the University of Wyoming stable isotope facility for analysis. It is important to note that this method of preparation measures the C- and O-isotopic composition of carbonate minerals in the bulk rock sample, not as individual mineral separates. The stable-isotope results are reported as $\delta^{13}\text{C}$ and $\delta^{18}\text{O}$ in the usual ‰ (per mil, or parts per thousand) notation relative to the VPDB (Vienna PeeDee Belemnite) isotopic standard. Unfortunately, samples from within the USZ itself had insufficient carbonate in them for isotopic analysis.

2.5. Assay Data

Tintina provided assay data to the author for ore intercepts drilled during the 2010-2011 campaign. These analyses were performed by ALS Chemex. A suite of 33 elements was quantified by the “four acid/ICP-AES multi-element package”. Gold concentrations were determined by fire assay and atomic absorption spectroscopy (AAS), with an effective range of 0.005-10 ppm. Barium was quantified by fusion/X-Ray fluorescence (XRF).

3. Results

3.1. Core Samples

Although many of the micro-textures are too small to see with raw drill core, some larger pyrite laminations and gangue mineral textures are frequently best seen on the scale of drill core. Samples of cut drill core showing some examples of these textures are shown in Figure 6. Good examples of laminated, semi-massive to massive sulfide ore are shown in Figures 6A, 6B, and 6C. These samples show evidence of soft-sediment deformation, as well as diagenetic recrystallization of sulfide minerals. Figure 6D is an example of a Newland Formation debris flow, with rounded to angular clasts of siliceous sediment with hydrothermal chalcopyrite replacing the matrix between the clasts. Figures 6E and 6F show interesting gangue mineral textures, consisting of coarse dolomite crystals rimmed by sulfides (LSZ) and feathery, non-oriented barite crystals (USZ). Although these two photographs are representative of the overall abundance of dolomite and barite in the LSZ and USZ, respectively, most of the time these gangue minerals are much finer-grained.

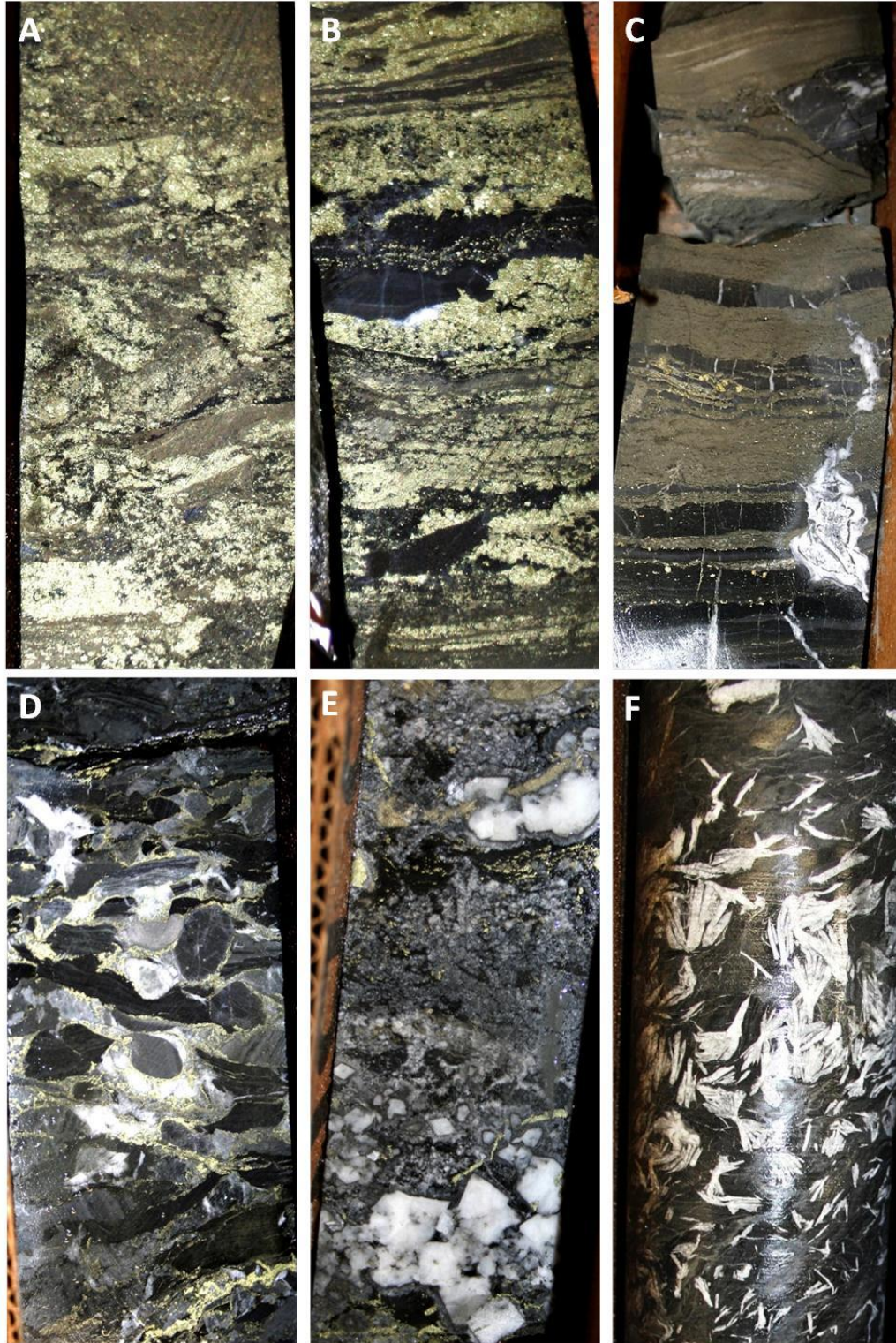


Figure 6: Photographs of Drill Core

(A and B) Chalcopyrite replacing deformed pyrite laminations. (C) Deformed pyrite laminations. (D) Silicified debris flow (some clasts contain laminated pyrite), with later chalcopyrite deposition in pore spaces. (E) Coarse, euhedral dolomite crystals with weak Cu mineralization (LSZ). (F) Feathered barite (USZ). Core is 2.5 inches in diameter.

3.2. Microscopy and SEM

3.2.1. Iron Sulfide Minerals

The primary sulfide mineralization at Black Butte is pyrite with some marcasite, and is very laterally extensive. The USZ is a nearly continuous zone of pyrite that has a strike length of 15 miles and extends nearly 5 miles south of the Volcano Valley Fault (Zieg and Leitch, 1998). All of the Cu-rich massive sulfide mineralization is hosted exclusively within the pyrite horizons, but is spatially constrained to the vicinity of the Volcano Valley Fault in the Black Butte area.

Pyrite mineralization styles at Black Butte are widely varied. Petersen (1989) observed eleven distinct pyrite mineralization habits, while Himes and Petersen (1990) described six of the most important (Table 2 and Plate 1). Two more are described in this study including framboidal (Plate 2) and “microbial vent fauna” types (Plate 3). Marcasite, an important yet much less abundant iron sulfide, is found throughout both the USZ and LSZ in the vicinity of Black Butte (Plate 2).

Table 2: Pyrite Types

Type	Stage of Mineralization	Dimensions	Description
Micro	I	1-5 μm	Cubic and spherical forms.
Mini	I	>5, <25 μm	Anhedral to euhedral, optically homogeneous but typically chemically zoned.
Porous	I	25 μm – several mm	Round or elongate. In USZ, typically contains inclusions of chalcopyrite and tennantite and has holes.
Coalesced	I and II	25 μm – several mm	Similar to porous. Isolated pyrite cubes merge so as to be indistinguishable in the core of the clusters.
Veined	I and II	25 μm – several mm	Pyrite veined with chalcopyrite.
Spherulitic	I and II	500 μm	Dark cores may contain amorphous Co, Ni, and As rich material or tennantite and/or chalcopyrite.
Framboidal	I	50 μm – 200 μm	Spheres of pyrite comprised of individual mini euhedral pyrite crystals.
Microbial Fauna	I	>1 mm	'Hoops' of pyrite grains filled with quartz or chalcopyrite.
Coarse Euhedral	II	25 μm – several mm	Distinct pyrite crystals showing either cubic or pyritohedron habit.

For the purposes of this study the pyrite has been broken down into two larger categories: pyrite I and pyrite II. Pyrite I represents initial (syngenetic) mineralization while pyrite II corresponds to later (epigenetic) Stage II mineralization (discussed in Section 4.1), during which the formation of the distinct siegenite-tennantite intergrowths (described below) occurred.

Although some of the various types of pyrite may correspond to either stage of mineralization, there are two distinct varieties that define each (Tables 2 and 3). Pyrite I is defined by porous pyrite that contains Cu/Co/Ni/As impurities. Porous pyrite with elevated metal impurities was observed at Black Butte before the identification of any discrete cobalt minerals (Zieg et al., 1991, Himes and Petersen, 1990). In this study, pyrite I was found to vary in composition spatially throughout the deposit according to the overall assay of the rock. For example, in areas with high Cu but low Co-Ni assays, the porous pyrite had elevated Cu but low

or undetected Co and Ni. Conversely, in zones rich in Co and Ni, the early pyrite was found to be enriched in Co, Ni, and As, as well as Cu. Overall, there is a very tight correlation between (Co + Ni) and As within the Black Butte ore body (discussed below).

Pyrite II is defined as pyrite that formed during Stage II mineralization. It has a relatively pure composition and is most frequently either euhedral or coalesced (Plate 1). Pyrite II likely formed from the dissolution and reprecipitation of pyrite I, during which process most of the impurities were removed. The transport distance of the impurities (Cu, As, Co, Ni) leached from pyrite I is believed to have been quite small based upon the observation that these metals frequently form secondary minerals (tennantite, siegenite) within close proximity to the pyrite from which they were leached.

The relationship between pyrite I and pyrite II is clearly illustrated in photomicrographs A and B in Plate 2. The impure pyrite I, containing other metal impurities, is cut by a vein of Stage II chalcopyrite. Along the contact, the impure pyrite I has been converted to pure pyrite II. The pyrite II appears slightly brighter in reflected light, but darker in the SEM-BSE image (Plate 2B). The latter observation is explained by the lower average atomic mass of pyrite II, due to the absence of heavy-metal impurities.

Marcasite, which is easily distinguishable from pyrite based on its optical anisotropy, occurs in both sulfide horizons and seems to play an important role in the formation of a Stage I cobalt mineral, alloclasite. It can be found alongside siegenite and copper minerals as well as with pyrite in regions barren of economic metals. The deposit also exhibits examples of pyrite after marcasite. Photomicrograph E from plate 2 depicts a pyrite spheroid which exhibits distinct characteristics of pyrite after marcasite including: 1) two pyrite orientations from one marcasite parent crystal exhibiting distinct anisotropy, 2) numerous small pores along grain twin

boundaries, and 3) no pore filling (Murowchick, 1992). Although marcasite is a common alteration product of pyrrhotite in many sulfide mineral deposits, not a single grain of pyrrhotite was found in this study. Because marcasite is metastable relative to pyrite, it is thermodynamically impossible for marcasite to form by replacement of pre-existing pyrite. These two observations mean that most if not all of the marcasite at Black Butte probably deposited directly from solution as orthorhombic FeS₂, rather than replacing pre-existing Fe-sulfides.

Table 3: EMPA Analyses of Pyrite Grains

Analysis	S	Cu	Ag	Fe	Zn	Co	Ni	Pb	As	Bi	Sb	Au	Total
	Elemental Percent												
Py-I 1	46.425	0.267	0.030	37.953	<0.07	3.909	0.674	0.444	6.045	2.389	0.125	<0.02	98.245
Py-II 1	50.602	0.729	<0.009	45.039	<0.07	0.275	0.124	0.122	0.069	0.157	<0.03	0.008	96.998
Py-II 2	51.864	0.098	<0.009	44.677	0.017	0.375	0.083	0.596	0.192	0.174	<0.03	0.017	98.098
Py-II 3	50.760	0.885	0.005	44.639	0.023	0.319	0.202	0.154	0.067	<0.1	<0.03	0.012	97.020
Py-II 4	54.051	0.068	0.005	46.210	<0.07	0.081	<0.03	0.780	0.037	<0.1	<0.03	0.004	101.085
Py-II 5	52.843	0.041	0.002	45.545	<0.07	0.053	0.020	1.477	<0.027	<0.1	<0.03	0.015	99.814
	Atomic Percents												
Py-I 1	62.821	0.182	0.012	29.486	-0.004	2.878	0.498	0.093	3.501	0.496	0.045	0.000	100.000
Py-II 1	65.658	0.477	0.000	33.552	-0.004	0.194	0.088	0.024	0.038	0.031	-0.004	0.002	100.000
Py-II 2	66.469	0.064	0.001	32.874	0.011	0.261	0.058	0.118	0.105	0.034	0.001	0.004	100.000
Py-II 3	65.772	0.578	0.002	33.209	0.015	0.225	0.143	0.031	0.037	-0.001	-0.004	0.003	100.000
Py-II 4	66.943	0.042	0.002	32.859	-0.004	0.054	-0.003	0.149	0.019	-0.004	-0.004	0.001	100.000
Py-II 5	66.688	0.026	0.001	33.000	-0.004	0.036	0.014	0.289	0.004	-0.004	-0.004	0.003	100.000

*Result was below the limit of quantification. Specimen locations: Py-I 1 = SC10-05 411.8m (LSZ); Py-II 1,2 = SC10-05 411.8m(LSZ); Py-II 3 = SC11-018 73.5m (USZ); Py-II 4,5 SC10-06 275.84m (LSZ).

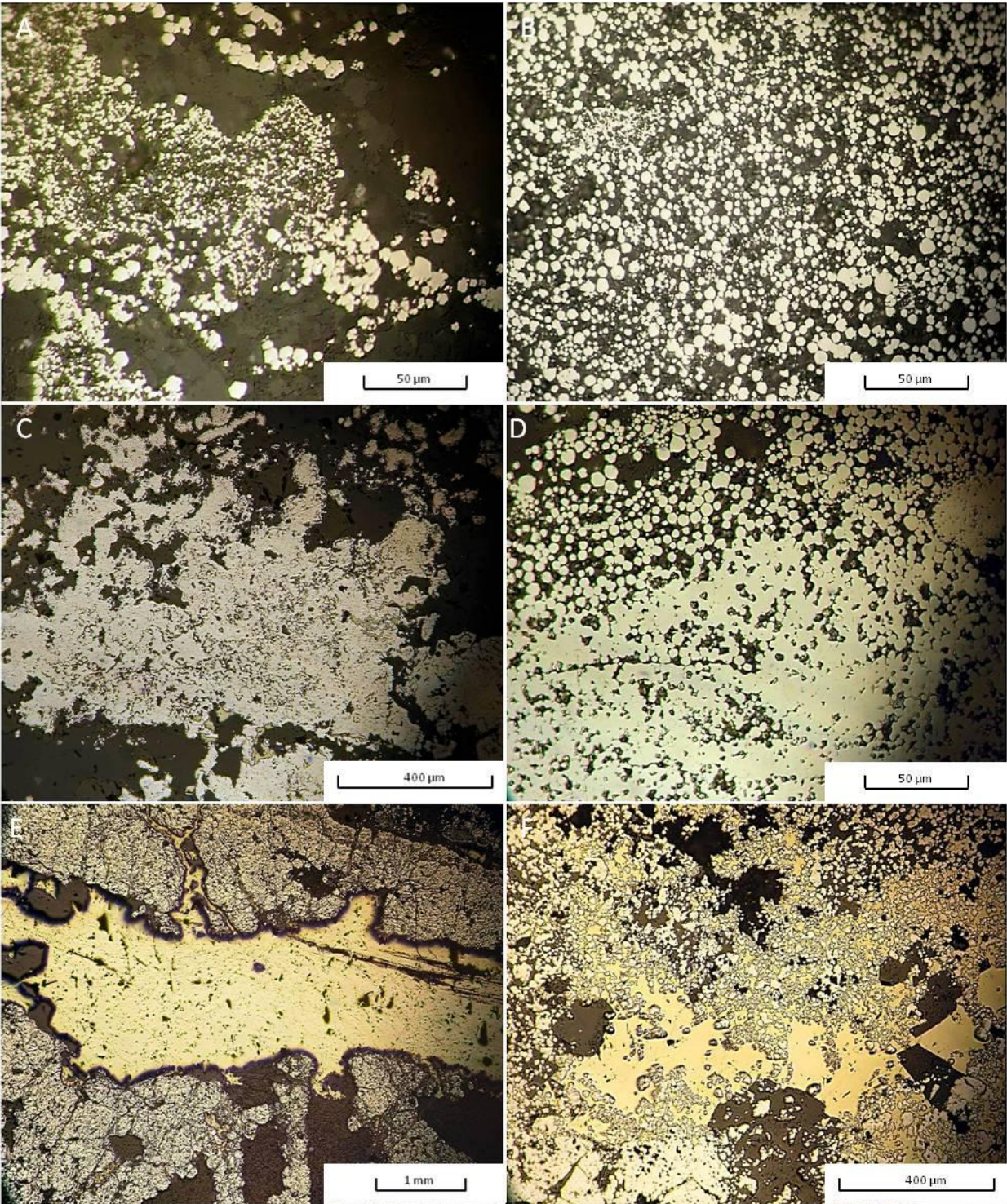


Plate 1: Pyrite Types

A) Micro pyrite from USZ; B) Mini pyrite from USZ; C) Porous pyrite with intergrown chalcopyrite from USZ; D) Coalesced pyrite from USZ; E) Veined chalcopyrite from LSZ; F) Veined chalcopyrite from USZ. All images are optical photomicrographs.

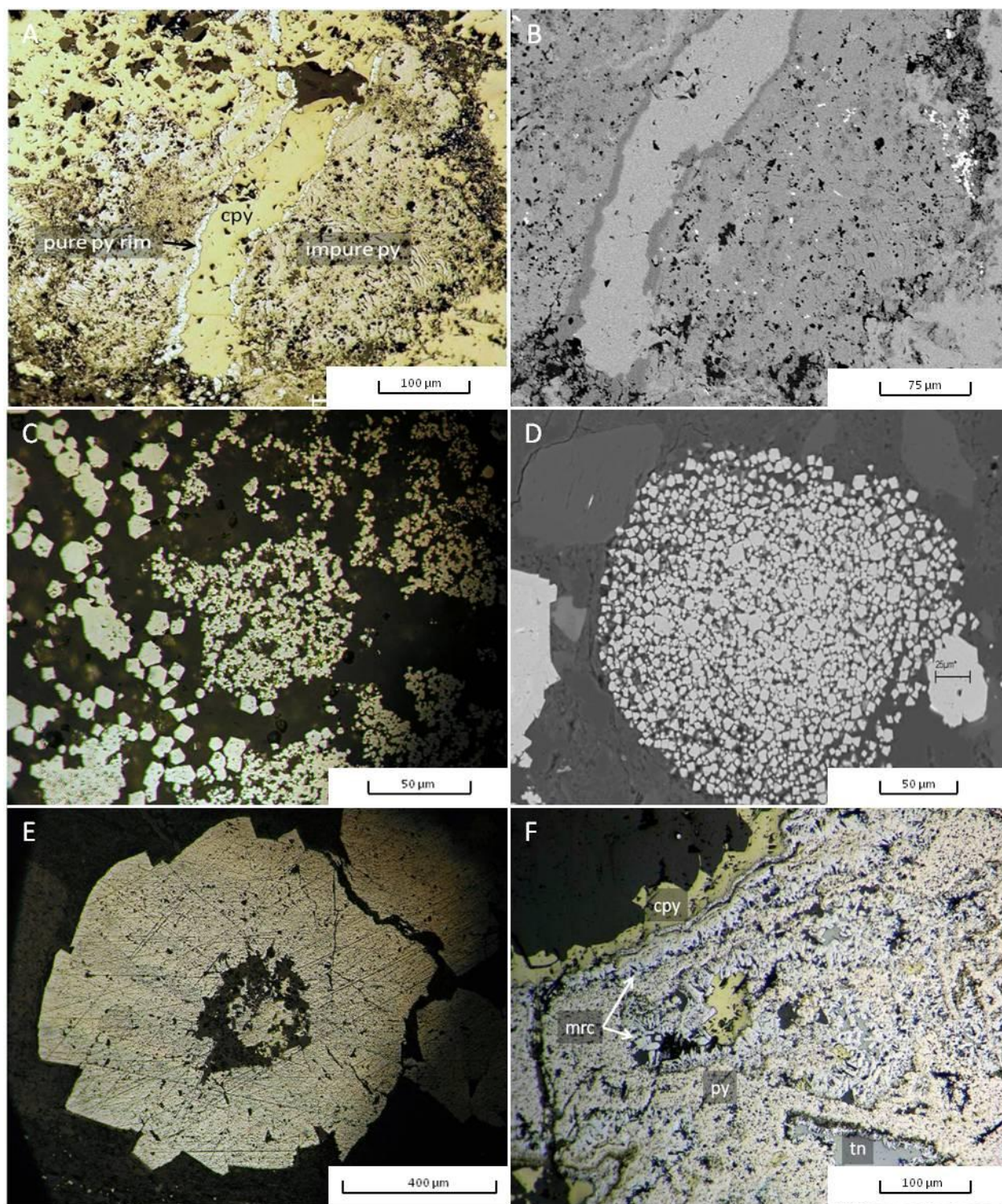


Plate 2: Other Iron Sulfides

A) Optical photomicrograph of chalcopyrite vein rimmed by pure pyrite II and surrounded by impure pyrite I from LSZ; B) SEM-BSE image of same chalcopyrite vein; bright spots are bismuthinite and galena; C) Optical photomicrograph of pyrite framboid D) SEM-BSE image of USZ pyrite framboid; E) Optical photomicrograph of pyrite spheroid from USZ with quartz core; F) Optical photomicrograph of intergrown pyrite and marcasite from USZ.

3.2.1.1. Microbial Fauna

Black Butte contains a unique set of pyrite features that have been interpreted to be Precambrian microbial fauna (McGoldrick and Zieg, 2004, Plate 3). The tentative identification is from a personal communication between Gerald Zieg of Tintina Resources and Dr. Jack Farmer, an astrobiologist from NASA who has examined the specimens. Although the findings from Black Butte are not published in the literature, Precambrian microbial fossils have been reported from the Newland Formation at other locations (Schieber, 2007).

Found throughout both continuous ore horizons, these unique pyrite formations are elliptical or circular and between 1 and 3 mm in diameter. These structures are theorized to have formed from pyrite replacement of original biofilm. The microbes may have assembled together in microbial mats or tubes and were subjected to rapid burial preserving them. The importance to this study is that both copper and cobalt mineralization have been found inside the forms. Epitaxial overgrowths of alloclasite on marcasite (described below) have only been observed within the confines of these structures in the LSZ (Plate 5). Often, the sulfide hoops are concentrically zoned, with distinct layers of porous pyrite, marcasite, and chalcopyrite (Plate 3E). The surrounding gangue is mainly quartz, but also includes minor barite and Ba-feldspar.

The origin of these structures is not fully understood. Today, microbial vent fauna are found in abundance in and around both black smokers ($T > 250^{\circ}\text{C}$) and white smokers ($T < 200^{\circ}\text{C}$) on the seafloor. These chemosynthetic bacteria utilize oxygen and sulfide for energy (Childress and Fischer, 1992) and thrive in the complete absence of sunlight (Le Bris et al., 2003). It seems possible that the circular sulfide aggregates represent vertical tubes of biofilm that either served as a substrate for direct precipitation of pyrite/marcasite, or that were later replaced by pyrite/marcasite. Although it is possible that the textures could have formed by abiotic processes, the unique and unusual shapes suggest an unusual and unique origin.

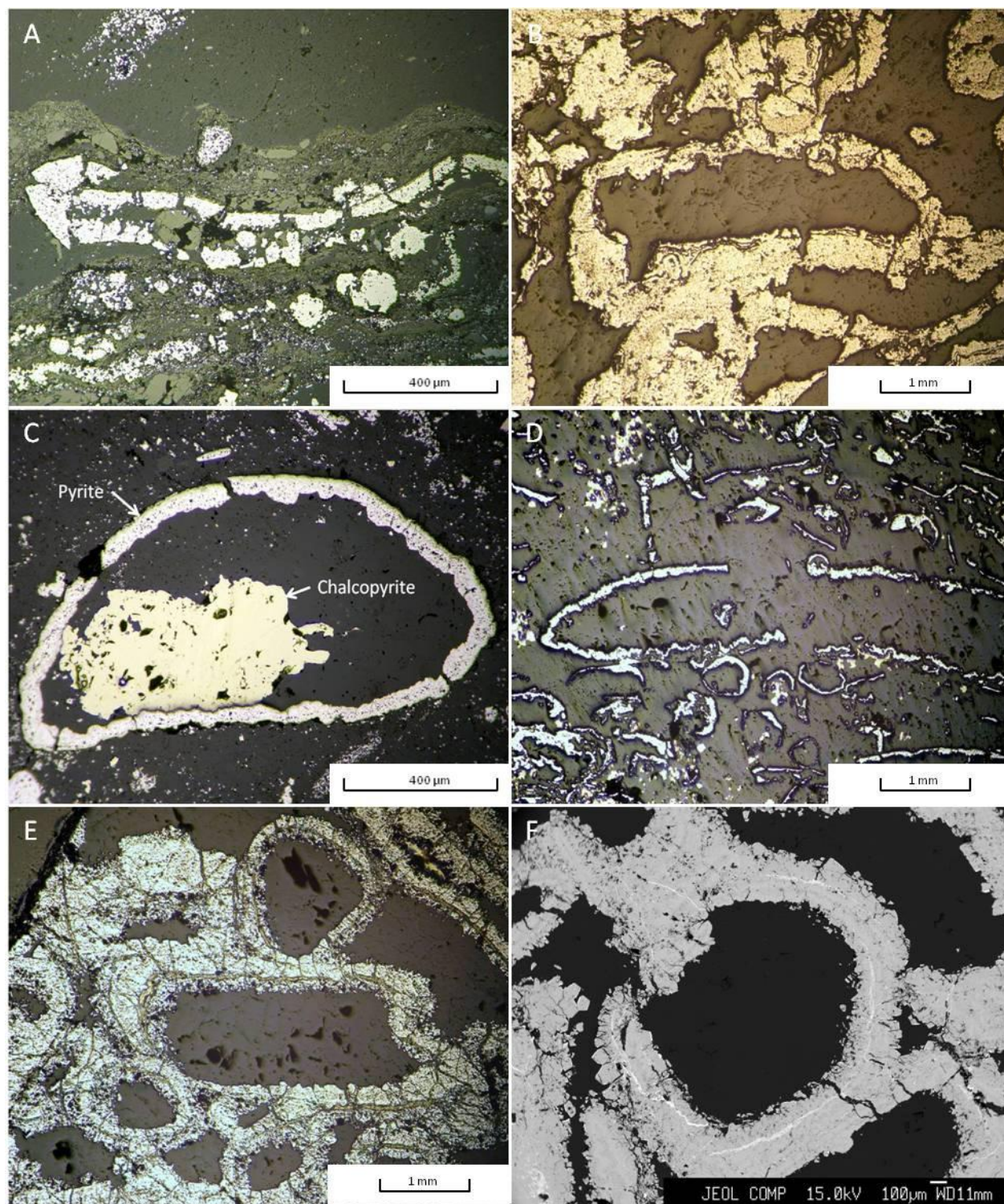


Plate 3: Pyrite "Vent Fauna"

A) Pyrite 'vent fauna' type structure with atypical form from USZ; gangue is quartz and hydrothermal feldspar, dark gangue is graphite; B) Typical 'vent fauna' structure from USZ; C) 'Vent' type structure controlling chalcopyrite mineralization from USZ; D) 'Vent fauna' structures of varying orientations from USZ; E and F) Reflected light and EMPA-BSE images of pyrite/marcasite 'vent fauna' structures containing central rings of chalcopyrite (yellow in E, white in F) from LSZ. All images except "F" are reflected light optical photomicrographs.

3.2.2. Copper Mineralization

The primary economic metal at Black Butte is copper. Textural evidence suggests that copper, in the form of chalcopyrite, deposited at all stages of mineralization. Early, Stage I chalcopyrite can be seen to coincide with porous pyrite and marcasite, whereas later, Stage II chalcopyrite veins replace pre-existing sulfides, and are associated with pure pyrite II and Stage II siegenite and tennantite (Plate 4).

Chalcopyrite has a variety of mineralization styles. These include: 1) disseminated grains scattered through fine-grained, clastic sediment; 2) laminated bands parallel to bedding; 3) discrete layers within zoned “vent fauna” textures; 4) irregular-shaped masses surrounding and replacing pre-existing pyrite and marcasite; and 5) veins or small breccia bodies cutting the stratiform ore and surrounding wallrock. Types 1, 2, and 3 are assumed to be part of Stage I mineralization (syngenetic), whereas Types 4 and 5 are mainly Stage II (epigenetic). Type 4 is probably the most abundant form of chalcopyrite throughout Black Butte. Two EMPA analyses of this type of chalcopyrite show trace but detectable levels of impurities, including Ag, Co, Ni, and As (Table 4). Chalcopyrite also frequently occurs as infilling within the central void of the “vent fauna” structures (Plate 3C). Finally, chalcopyrite has been observed as small inclusions within sphalerite (i.e., “chalcopyrite disease”) (Plate 9). Previous studies (e.g., Barton and Bethke, 1987) have shown that chalcopyrite disease is a replacement reaction in which chalcopyrite grains nucleate and grow around Fe impurities in the host phase. At Black Butte, this reaction probably occurred during Stage II mineralization.

In addition to chalcopyrite, copper mineralization has been observed to occur as tennantite, bornite, chalcocite, and enargite. Tennantite is a common mineral at Black Butte and occurs in all sulfide zones. It is often found in close association with Stage II chalcopyrite and

siegenite. Based on numerous SEM-EDS analyses, tennantite at Black Butte is essentially devoid of Sb, and can be approximated by the formula: $(\text{Cu,Fe})_{12}\text{As}_4\text{S}_{13}$ (Table 5). Higher-resolution EMPA analyses show trace quantities of impurities, including Ag, Co, and Ni. One sample of a late, sphalerite-rich vein contained tennantite that was unusually rich in Zn and Bi (Table 5, analyses 4 and 5). In this case, the Zn appears to have substituted for Cu + Fe, and the Bi for As.

Compared to chalcopyrite and tennantite, the other Cu-bearing sulfides are rare, and appear to be restricted to the USZ where they typically occur together in late veins or pore-fillings. Interestingly, bornite, chalcocite, and enargite are all minerals that are characteristic of a high $a\text{S}_2$ environment (Barton and Skinner, 1979).

Table 4: EMPA analyses of Chalcopyrite Grains

Analysis	S	Cu	Ag	Fe	Zn	Co	Ni	Pb	As	Bi	Sb	Au	Total
	Elemental Percent												
1	34.062	33.904	0.005	29.338	0.050	0.037	<0.03	0.075	0.026	0.026	<0.03	<0.02	97.426
2	33.885	33.763	0.008	28.899	<0.07	0.142	0.116	0.075	0.071	0.017	<0.03	<0.02	96.917
	Atomic Percents												
1	50.048	25.136	0.002	24.750	0.036	0.030	-0.004	0.017	0.016	0.006	-0.004	-0.002	100.000
2	50.064	25.170	0.003	24.514	-0.004	0.114	0.094	0.017	0.045	0.004	-0.004	-0.003	100.000

*Result was below the limit of quantification. Specimen locations: 1 = SC10-05 411.8m (LSZ); 2 = SC11-018 73.5m (USZ).

Table 5: EMPA Analyses of Tennantite Grains

Analysis	S	Cu	Ag	Fe	Zn	Co	Ni	Pb	As	Bi	Sb	total
	weight percent											
1	27.274	44.697	0.018	5.829	0.115	0.564	0.232	0.060*	19.693	0.266	0.004*	98.749
2	27.173	45.578	0.010	4.744	0.207	0.229	0.052	0.030*	19.667	0.373	0.095	98.142
3	27.570	45.291	0.008*	4.900	0.144	0.288	0.085	0.096	19.575	0.388	0.100	98.431
4	25.942	39.042	<0.01	1.691	6.824	0.088	<0.03	0.033*	16.226	7.430	0.088	97.356
5	26.333	40.692	<0.01	1.052	7.188	0.285	0.064	0.134	16.961	6.403	0.153	99.247
	atomic percent											
1	43.886	36.289	0.009	5.385	0.091	0.494	0.204	0.015	13.561	0.066	0.002	100.000
2	44.074	37.302	0.005	4.418	0.164	0.202	0.046	0.008	13.652	0.093	0.041	100.000
3	44.476	36.867	0.004	4.538	0.114	0.253	0.075	0.024	13.515	0.096	0.043	100.000
4	44.637	33.897	0.000	1.670	5.759	0.082	-0.003	0.009	11.949	1.961	0.040	100.000
5	44.269	34.517	-0.001	1.015	5.927	0.261	0.058	0.035	12.203	1.652	0.068	100.000

*Result was below the limit of quantification. Specimen locations: 1, 2, 3 = SC11-018 73.5m; 4,5 = SC11-029 64.3m.

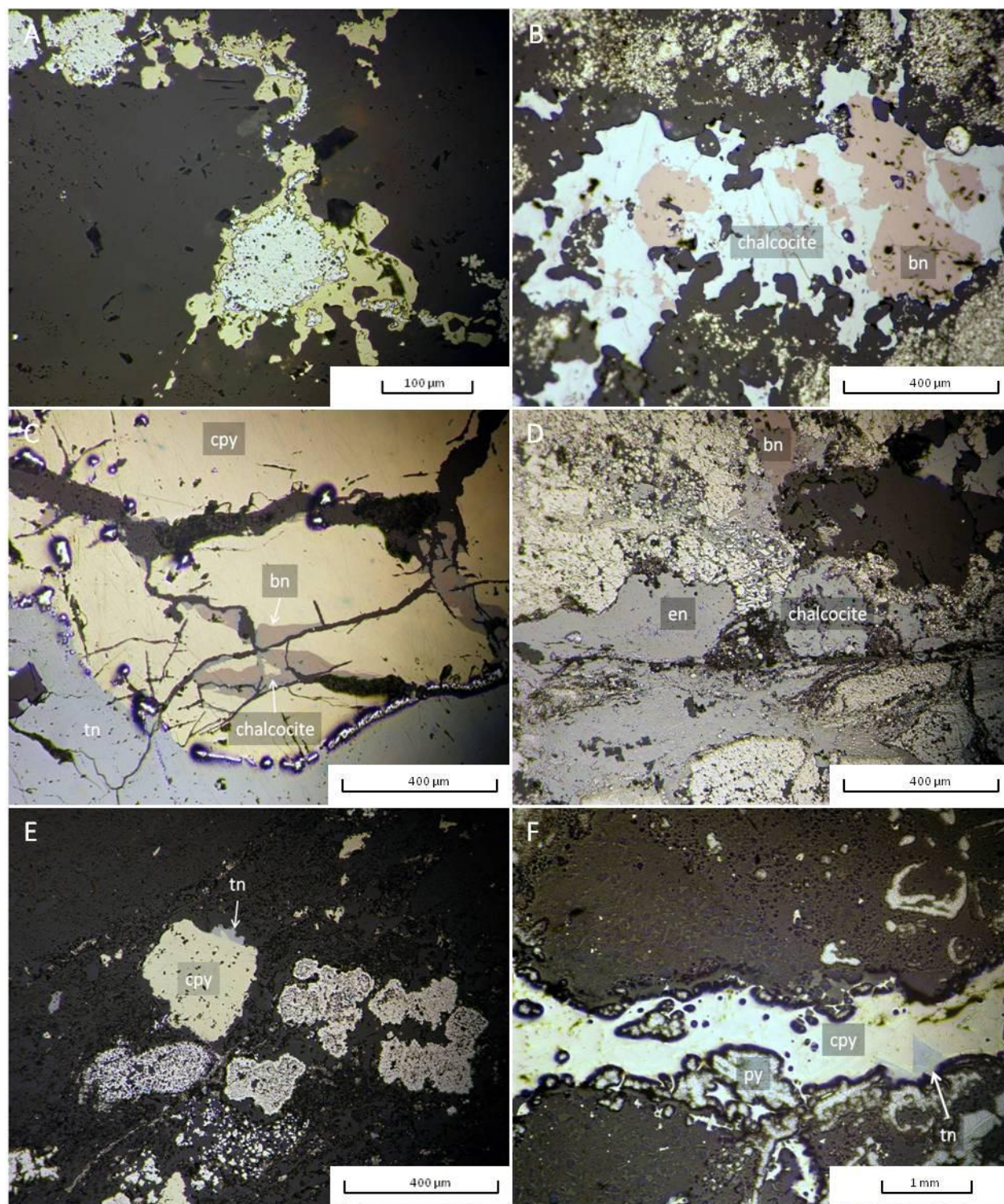


Plate 4: Copper Mineralization

A) Cpy rimming pyrite in USZ; B) Late chalcocite and bornite filling pore space in the USZ; C) Large cpy crystal containing small bornite and chalcocite veins adjacent to tennantite and separated by pure pyrite II; D) Bornite-chalcocite-energite vein cutting impure pyrite I in USZ; E) Isolated cpy grain with minor tennantite rim from USZ; F) Cpy vein with minor pure pyrite II and tennantite from USZ. All images are optical photomicrographs.

3.2.3. Cobalt/Nickel Mineralization

Cobalt is the second most important economic metal at Black Butte. Mineralization occurs throughout the entire deposit in both the USZ and LSZ. This study has found that cobalt, in a crystalline form large enough to observe with an optical microscope, occurs almost exclusively as the mineral siegenite. Siegenite, a thiospinel with the chemical formula $(\text{Co,Ni})_3\text{S}_4$, is named for the Siegen district in Germany and is not a common ore mineral (mindat.org). Most frequent impurities are either iron or copper, both of which are found in the siegenite crystals at Black Butte (Table 6). The siegenite crystals found in this study range from very small ($\sim 5\mu\text{m}$) rims on other minerals to euhedral prisms several mm in diameter. Some of the latter, first identified by Tintina geologists, are distinguishable with a hand lens. Under reflected light, siegenite has a creamy-white color with a slight pinkish hue, and is isotropic. It is whiter than tennantite, with which it is commonly intergrown. Siegenite is actually more difficult to identify with an SEM due to having an average atomic mass very close to chalcopyrite. On a grayscale BSE image, the mineral boundaries between siegenite and chalcopyrite can be indistinguishable unless the contrast is very finely adjusted (Plate 7b).

Siegenite, along with other cobalt sulfides including carrollite (CuCo_2S_4), linnaeite (Co_3S_4), cobaltite (CoAsS), glaucodot (CoAsS), alloclasite (CoAsS), and skutterudite ($(\text{Co,Fe})\text{As}_{2-3}$), can be difficult to identify under a microscope due to the similarity of optical properties with pyrite and marcasite (Himes and Petersen, 1990). This is especially true with very small mineral grains. The alloclasite identified in this study (Plate 5) is a prime example of this; optically it is nearly indistinguishable from the surrounding pyrite.

During the course of their electron microprobe study of USZ ore, Himes and Petersen (1990) confirmed the presence of minute crystals of unidentified Co-Ni-As-S phases, which they

believed were cobaltite, although other phases such as siegenite, glaucodot, or alloclasite may also have been present. The cobalt minerals observed were very small ($<5\mu\text{m}$), however, and difficult to identify optically. Zieg et al. (1991) had not identified any distinct cobalt minerals, but suggested that the mineralization was primarily cobaltite or glaucodot.

Although siegenite is the primary cobalt mineral identified in this study, assay data suggest that it was not the first Co-bearing mineral to form at Black Butte (Section 3.2).

Based on EMPA analyses, the siegenite within the Black Butte deposit has an average chemical formula approximated by $(\text{Co}_{0.43}\text{Ni}_{0.44}\text{Fe}_{0.064}\text{Cu}_{0.062})_3\text{S}_4$. All of the crystals analyzed in this study are plotted on a compositional diagram in Co-Cu-Ni-Fe-S space in Figure 7 (data from Table 6 and appendix B). As this plot shows, most of the analyses obtained in this study are close to siegenite analyses reported by previous workers (see Craig et al., 1979, and references therein), and tend to be slightly enriched in Ni relative to Co, with variable but small amounts of Cu and Fe.

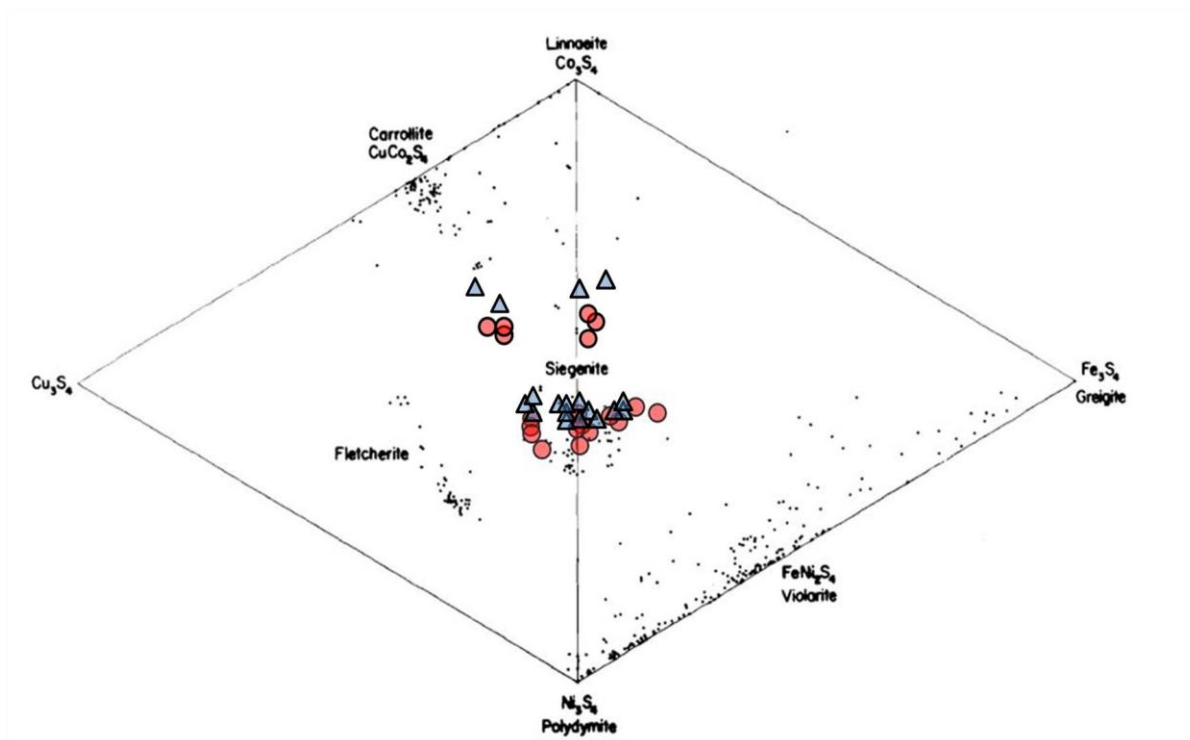


Figure 7: Black Butte Siegenite Analyses

Plotted on the Co-Ni-Cu-S and Co-Ni-Fe-S ternary systems. Red circles are SEM/EDX analyses, blue triangles are EMPA analyses. Small black dots show analyses from previous workers (from Craig et al., 1979).

Table 6: EMPA Analyses of Siegenite Grains

Analysis	S	Cu	Ag	Fe	Zn	Co	Ni	Pb	As	Bi	Sb	Au	total
	weight percent												
1	42.411	0.477	0.001*	5.302	<0.07	23.403	27.634	0.078*	<0.028	<0.1	<0.03	<0.02	99.226
2	42.041	0.470	0.004*	5.574	<0.07	23.144	27.835	0.070*	<0.028	<0.1	<0.03	<0.02	99.063
3	42.066	0.434	0.007*	5.558	<0.07	23.057	27.361	0.081*	<0.028	<0.1	0.016*	<0.02	98.475
4	41.809	0.413	<0.009	5.557	<0.07	23.404	27.383	0.130	<0.028	<0.1	<0.03	<0.02	98.696
5	42.025	0.386	0.002*	4.732	<0.07	22.741	28.307	0.049*	<0.028	<0.1	<0.03	<0.02	98.192
6	41.358	5.724	<0.009	1.342	-0.166	23.133	26.744	0.173	<0.029	<0.1	0.004*	<0.02	98.308
7	41.414	5.551	0.002*	0.611	<0.07	23.356	26.984	0.100	0.022*	<0.1	<0.03	<0.02	98.017
8	41.532	5.694	<0.009	0.664	<0.07	22.813	26.977	0.065*	0.044	<0.1	<0.03	<0.02	97.724
9	40.406	9.096	0.004*	0.666	0.026*	30.967	16.291	0.067*	0.098	<0.1	<0.03	-0.020	97.503
10	40.837	12.895	0.001*	2.888	<0.07	29.668	13.363	0.167	0.089	0.049*	<0.03	-0.008	99.898
	atomic percent												
1	57.739	0.328	0.000	4.145	-0.004	17.335	20.546	0.016	0.000	-0.003	0.002	-0.004	100.101
2	57.462	0.324	0.002	4.374	-0.004	17.211	20.778	0.015	-0.002	-0.004	-0.004	0.001	100.153
3	57.730	0.300	0.003	4.379	-0.004	17.215	20.507	0.017	0.002	-0.004	0.006	0.001	100.153
4	57.427	0.286	-0.002	4.382	-0.004	17.490	20.541	0.028	-0.004	-0.004	-0.004	-0.003	100.134
5	57.880	0.268	0.001	3.742	-0.004	17.041	21.292	0.010	0.002	-0.004	-0.004	0.001	100.227
6	57.325	4.003	-0.002	1.068	-0.004	17.445	20.245	0.037	0.002	-0.004	0.001	0.001	100.118
7	57.600	3.896	0.001	0.488	-0.004	17.674	20.497	0.022	0.013	-0.004	-0.004	0.001	100.179
8	57.810	3.999	0.000	0.531	-0.004	17.276	20.508	0.014	0.026	-0.004	-0.004	0.001	100.154
9	56.774	6.449	0.002	0.537	0.018	23.673	12.501	0.015	0.059	-0.004	-0.004	-0.005	100.017
10	56.329	8.975	0.000	2.287	0.001	22.266	10.067	0.036	0.052	0.010	-0.004	-0.002	100.018

*Result was below the detection limit. Specimen locations: 1,2,3,4,5 = SC10-05 411.8 (LSZ); 6,7,8 = SC11-018 73.5m (USZ); 9,10 = SC11-029 64.3m (USZ).

Cobalt mineralization within the LSZ consists of coarse grained siegenite, fine grained alloclasite, and possibly cobaltite. Siegenite, the primary form of cobalt mineralization, is found both as distinct prismatic crystals and as amorphous coatings or replacements, similar to those seen in the USZ (plate 7). The distinct crystalline variety ranges in size from tens of micrometers to a millimeter in diameter, the latter easily seen with a hand lens. The siegenite in the LSZ is compositionally no different from the USZ samples, regardless of crystal form.

Alloclasite (and possible cobaltite) mineralization, believed to be early, is very fine grained (ranging from 10 μ m to <1 μ m) and found to have a variety of crystal habits. Identified with the electron microprobe at WSU, alloclasite can be found as epitaxial growth crystals along the margins of marcasite grains (Plate 5B, 5C, 5D) and as porous aggregates intergrown with pyrite (Plate 6B and 6D). Additionally, it may be found as inclusions within siegenite grains

(Plate 6C) and within chalcopyrite (Plate 6E, 6F), although the crystal form may be cobaltite in those locales. The alloclasite at Black Butte contains a variety of impurities (Table 7), including Bi, Pb, Cu, Sb, and Ag. This variation in composition is similar (with respect to both elemental impurities as well as content by atomic percent) to Pyrite I, which was co-precipitated during Stage I mineralization.

Table 7: EMPA Analyses of Alloclasite Grains

Analysis	S	Cu	Ag	Fe	Zn	Co	Ni	Pb	As	Bi	Sb	Au	total
	weight percent												
1	24.572	0.111	<0.01	9.047	<0.07	13.562	13.153	0.090	33.325	1.680	0.051	0.019*	95.590
2	25.000	0.418	0.010	10.582	<0.07	14.830	9.956	0.118	31.727	1.929	0.006*	<0.02	94.570
3	18.967	1.088	0.025	2.790	<0.07	23.967	7.840	0.182	42.914	0.795	0.006*	<0.02	98.566
4	19.409	0.042*	0.001*	2.796	<0.07	31.164	4.469	0.023*	42.010	0.065*	0.652	-0.004	100.497
5	20.113	<0.052	0.004*	2.830	<0.07	28.993	5.664	<0.09	41.511	<0.1	0.253	0.024	99.388
	atomic percent												
1	41.725	0.095	0.000	8.820	-0.004	12.529	12.198	0.024	24.218	0.438	0.023	0.005	100.071
2	42.623	0.359	0.005	10.358	-0.004	13.756	9.270	0.031	23.149	0.505	0.003	0.001	100.057
3	33.319	0.964	0.013	2.813	-0.004	22.906	7.521	0.049	32.263	0.214	0.003	0.001	100.063
4	33.140	0.036	0.001	2.741	-0.004	28.952	4.168	0.006	30.699	0.017	0.293	-0.001	100.049
5	34.446	-0.031	0.002	2.782	-0.004	27.016	5.298	0.004	30.425	-0.004	0.114	0.007	100.055

*Result was below the detection limit. Specimen locations: 1,2,3 = SC10-05 411.8m (LSZ); 4,5 = SC10-06 275.8m (LSZ).

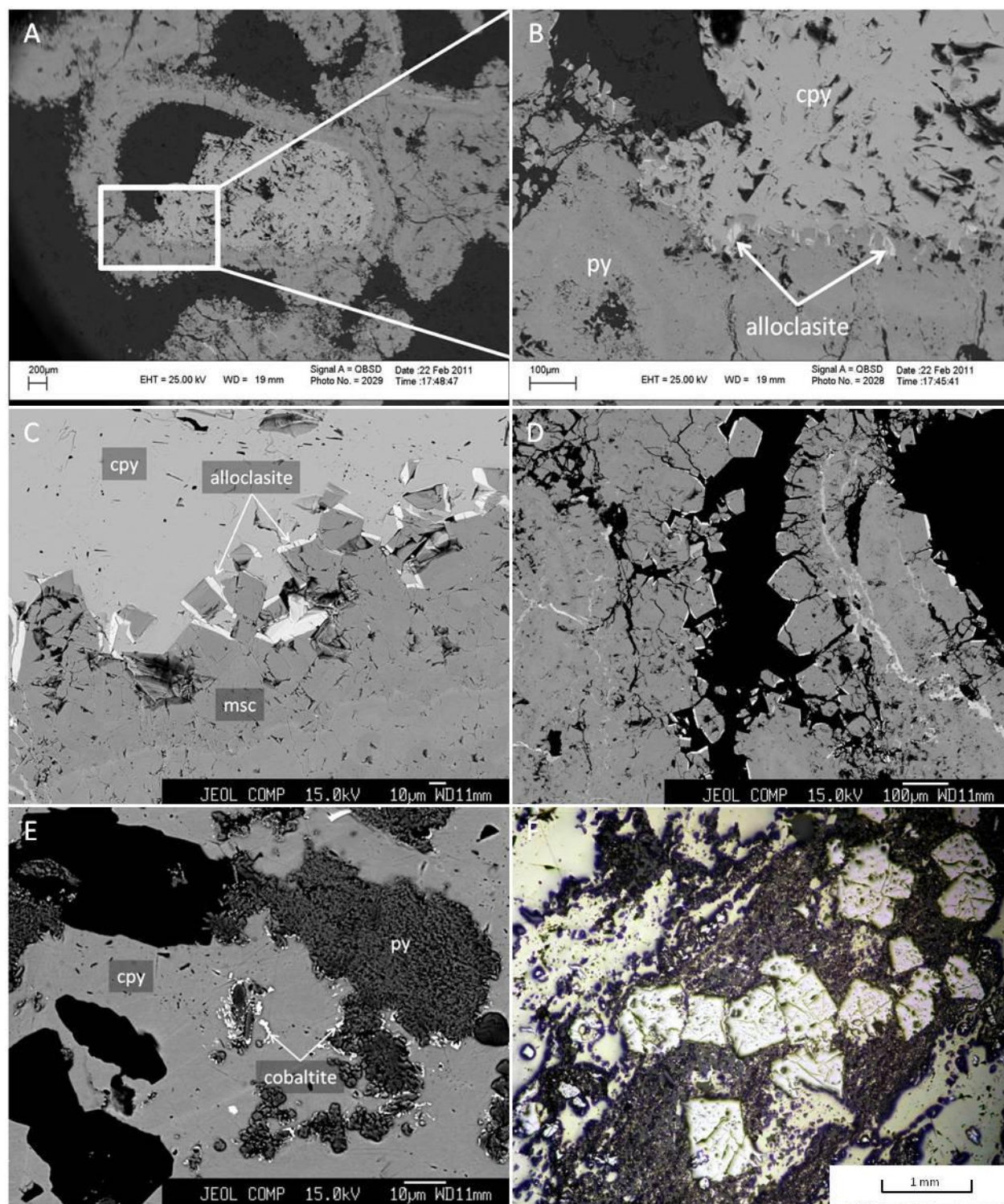


Plate 5: LSZ Cobalt Minerals I

A and B) SEM-BSE image showing alloclasite grains growing along marcasite grains along the boundary of a pyrite/marcasite 'vent fauna' structure and the chalcopyrite intergrowth; C) Greatly expanded EMPA-BSE image of alloclasite along marcasite grains showing epitaxial growth along two faces; D) EMPA-BSE image of alloclasite growing along marcasite into a quartz vein; E) EMPA-BSE image of cobaltite grains growing into chalcopyrite along the boundary of impure pyrite I; F) Optical photomicrograph of large euhedral siegenite crystals surrounded by apatite and chalcopyrite. Gangue is quartz and apatite.

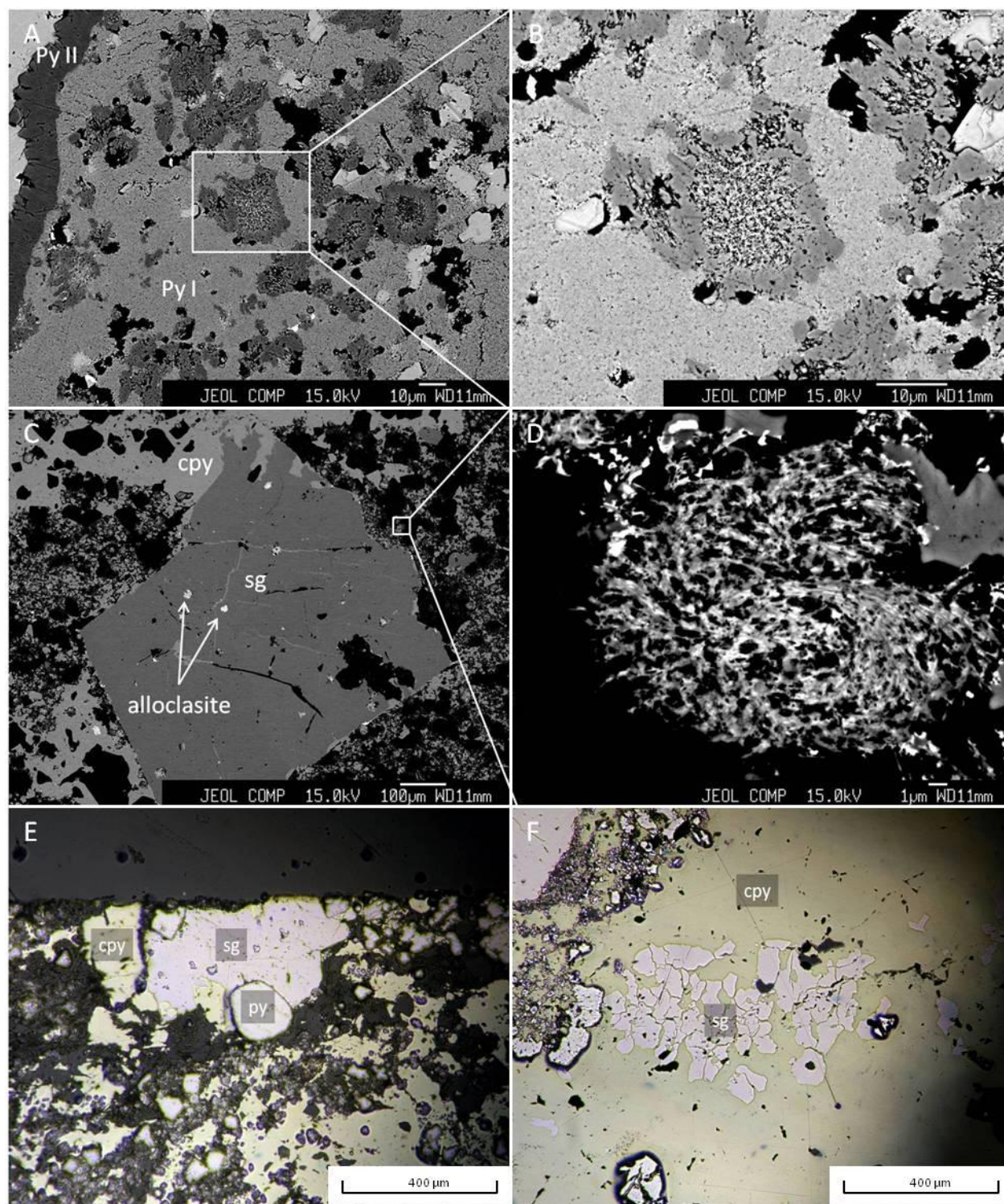


Plate 6: LSZ Cobalt II

A) EMPA-BSE image of impure pyrite I with zoned impurities; B) EMPA-BSE image of pyrite and alloclasite spheroid rimmed by pyrite; blown up from image A; C) EMPA-BSE image of siegenite grain with alloclasite or cobaltite inclusions and surrounded by pyrite and alloclasite spheroids grown in apatite gangue. D) Expanded image of alloclasite and pyrite spheroid surrounded by apatite; blown up from image C; E) Optical photomicrograph of siegenite and pyrite surrounded by chalcopyrite; gangue is quartz and apatite; F) Optical photomicrograph of siegenite grains intergrown with chalcopyrite.

In the USZ, Co and Ni have a different mineralization style than in the LSZ, which may be attributed to a stronger influence of Stage II ore fluids. This is shown by a distinct lack of alloclasite, and less impure Pyrite I (which has been observed in the USZ, but not containing Co or Ni impurities). Also, cobalt mineralization in the USZ, which occurs almost exclusively as siegenite, always is accompanied by tennantite. So much so, in fact, that unless tennantite is present, identification of siegenite crystals is nearly impossible. Siegenite in the USZ typically occurs as an amorphous coating with no distinct crystal habit (as opposed to the frequent discrete cubic grains observed in the LSZ), and is always coincident with tennantite. Siegenite is most frequently found along the margins of pyrite crystals, but has been noted to occur with tennantite as isolated mineral precipitates along the boundaries of quartz crystals (plate 7). In one instance, siegenite occurs with sphalerite in the USZ, but due to the low amount of zinc mineralization observed in the samples collected for this study, it is not known if this is an anomalous occurrence.

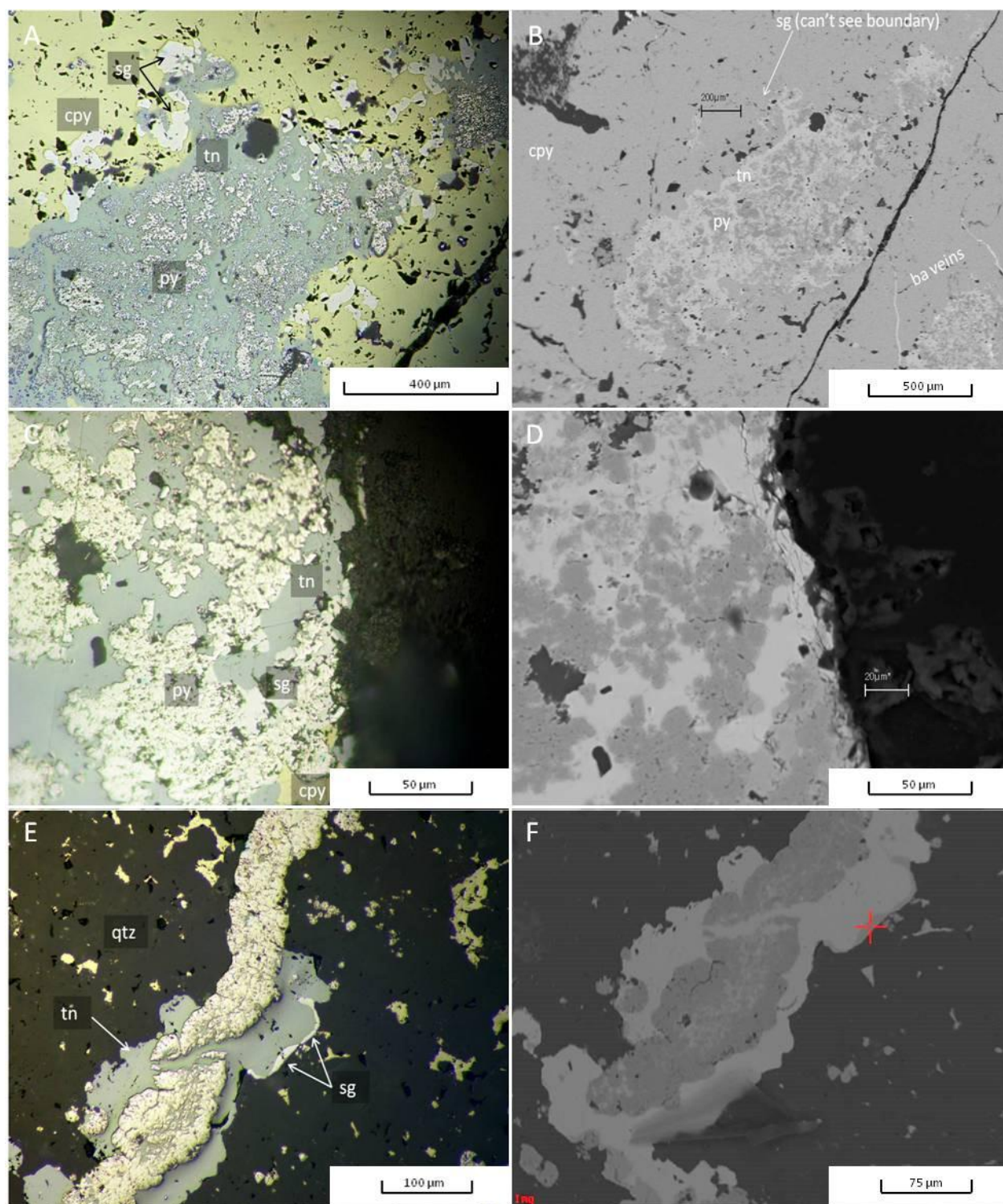


Plate 7: USZ Cobalt I

A and B) Optical photomicrograph and SEM-BSE image of tennantite, pyrite II, and siegenite contained within massive cpy. Tennantite (not easily seen) also contains very small galena inclusions. C and D) Optical photomicrograph and SEM-BSE image of tennantite, siegenite, and chalcopyrite crystals surrounded by pure pyrite II. E and F) Optical photomicrograph and SEM-BSE image of impure pyrite I surrounded by succeeding layers of pure pyrite II, tennantite, and siegenite.

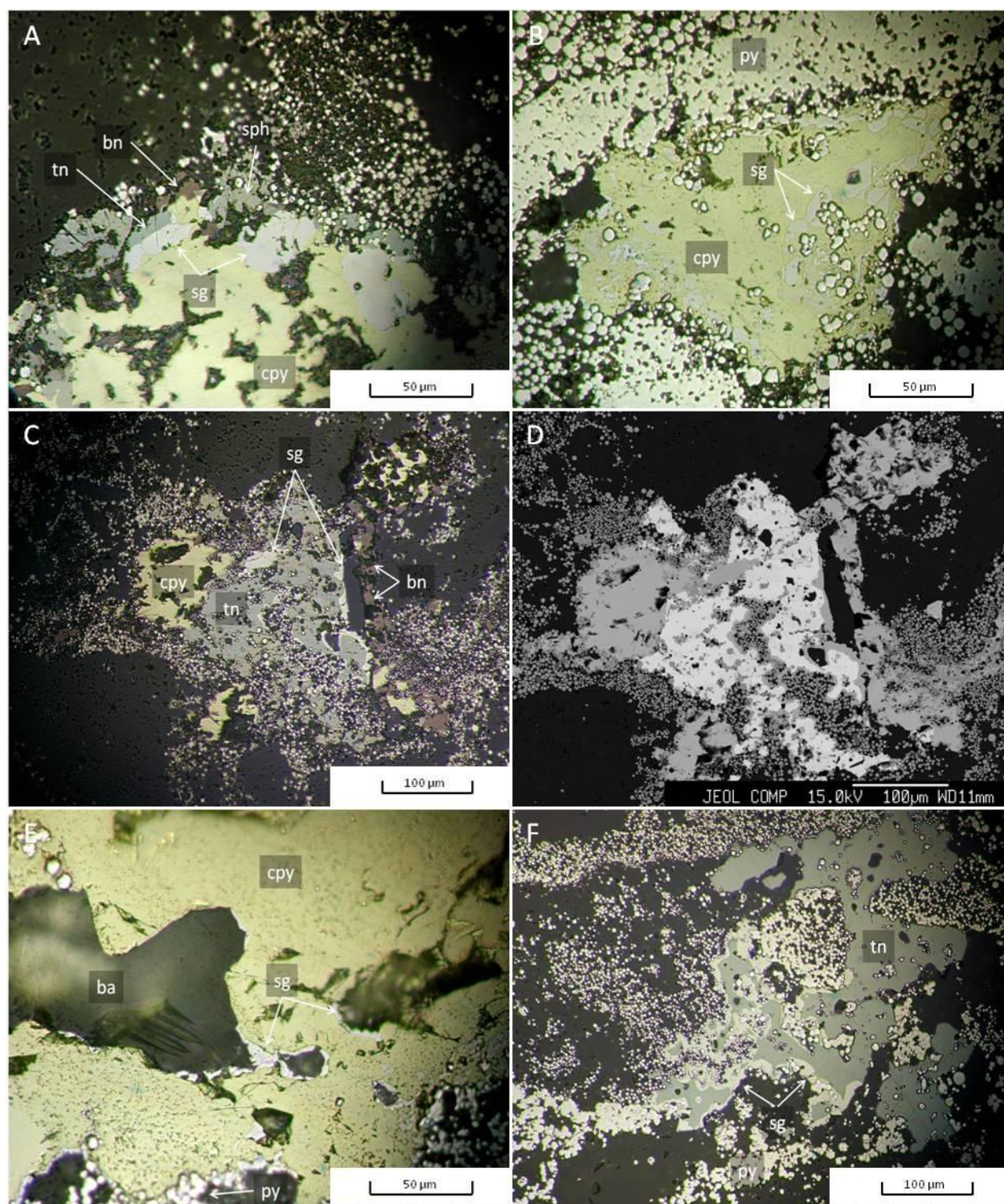


Plate 8: USZ Cobalt II

A) Unique mineral assemblage containing small euhedral pyrite II, sphalerite, bornite, cpy, and siegenite; B) Coalesced pyrite II surrounding cpy crystal containing siegenite crystals; C and D) Reflected and EMPA-BSE image of tennantite intergrown with cpy, bornite, and siegenite; E) Siegenite and pyrite II rimming the boundary between cpy and barite; F) Siegenite rimming tennantite surrounded by pyrite II hosted in quartz. All images (except D) are optical photomicrographs.

3.2.4. Pb, Zn, and Bi Mineralization

Although lead and zinc mineralization is weak at Black Butte, higher concentrations of sphalerite and galena have been noted in both ore zones. Galena occurs throughout the deposit primarily as small crystals surrounded by pyrite that are easily visible on a BSE grayscale. Infrequently, larger minerals which can be identified in hand sample occur as well (Plate 8). As discussed in section 3.3, minor amounts of silver have been noted as impurities in the galena found at Black Butte, and there is a correlation between lead and silver suggested by assay data (see below).

Sphalerite can be found in trace to minor amounts throughout both the USZ and LSZ at Black Butte, and is sometimes associated with tennantite. Also, when sphalerite is found to occur with tennantite, the tennantite becomes zinc-rich. Based upon this association with tennantite, much if not most of the sphalerite is believed to have been deposited during Stage II. Most of the sphalerite grains identified in this study were free of chalcopyrite inclusions, although one veinlet of coarse sphalerite was riddled with chalcopyrite disease. Analyses of 7 sphalerite grains that were free of chalcopyrite disease gave a range of Fe contents from 0.84 to 4.19 atomic %, with an average of 1.73 atomic % Fe.

Small inclusions of bismuthinite (Bi_2S_3) have been noted in the LSZ at Black Butte, and are easily identified on a BSE grayscale (Plate 2). A few tennantite grains were also found to be enriched in bismuth. Although economically unimportant, bismuthinite places important constraints on the conditions of Stage II mineralization, as discussed in section 4.2. Table 8 shows EMPA analyses of galena, sphalerite, and bismuthinite grains.

Table 8: EMPA Analyses of Galena, Sphalerite, and Bismuthinite Grains

Analysis	S	Cu	Ag	Fe	Zn	Co	Ni	Pb	As	Bi	Sb	Au	Total
	elemental percent												
GN 1	22.500	0.622	0.006*	12.425	<0.07	0.088	<0.03	67.469	0.017*	<0.1	<0.03	<0.02	97.215
GN 2	39.468	1.248	0.019	30.993	0.088*	0.277	0.049	34.528	0.026*	<0.1	<0.03	<0.02	103.422
SPH 1	32.423	1.057	<0.01	1.466	62.863	<0.027	<0.03	<0.09	<0.032	0.074*	0.038	<0.02	97.921
SPH 2	33.818	0.344	<0.01	4.827	59.865	0.005*	<0.03	0.091	0.014*	0.040*	<0.03	<0.02	98.943
Bi 1	16.128	2.004	<0.01	1.177	<0.07	0.416	0.283	3.038	0.189	73.035	0.038	0.017*	96.257
	atomic percents												
GN 1	56.920	0.795	0.004	18.048	-0.004	0.121	-0.004	26.414	0.018	-0.004	-0.004	0.001	100.000
GN 2	62.687	1.000	0.009	28.263	0.069	0.239	0.042	8.487	0.018	-0.004	-0.004	0.001	100.000
SPH 1	50.149	0.825	-0.005	1.302	47.692	-0.002	0.000	0.002	0.005	0.018	0.015	-0.001	100.000
SPH 2	51.137	0.263	0.001	4.191	44.402	0.004	-0.004	0.021	0.009	0.009	-0.004	0.000	100.000
Bi 1	53.860	3.377	0.001	2.256	-0.004	0.756	0.516	1.570	0.270	37.423	0.034	0.009	100.000

*Result was below the detection limit. Specimen locations: GN 1,2, SPH 2, and Bi 1 = SC11-024 170.7m (USZ); SPH 1 = SC10-05 411.8m (LSZ).

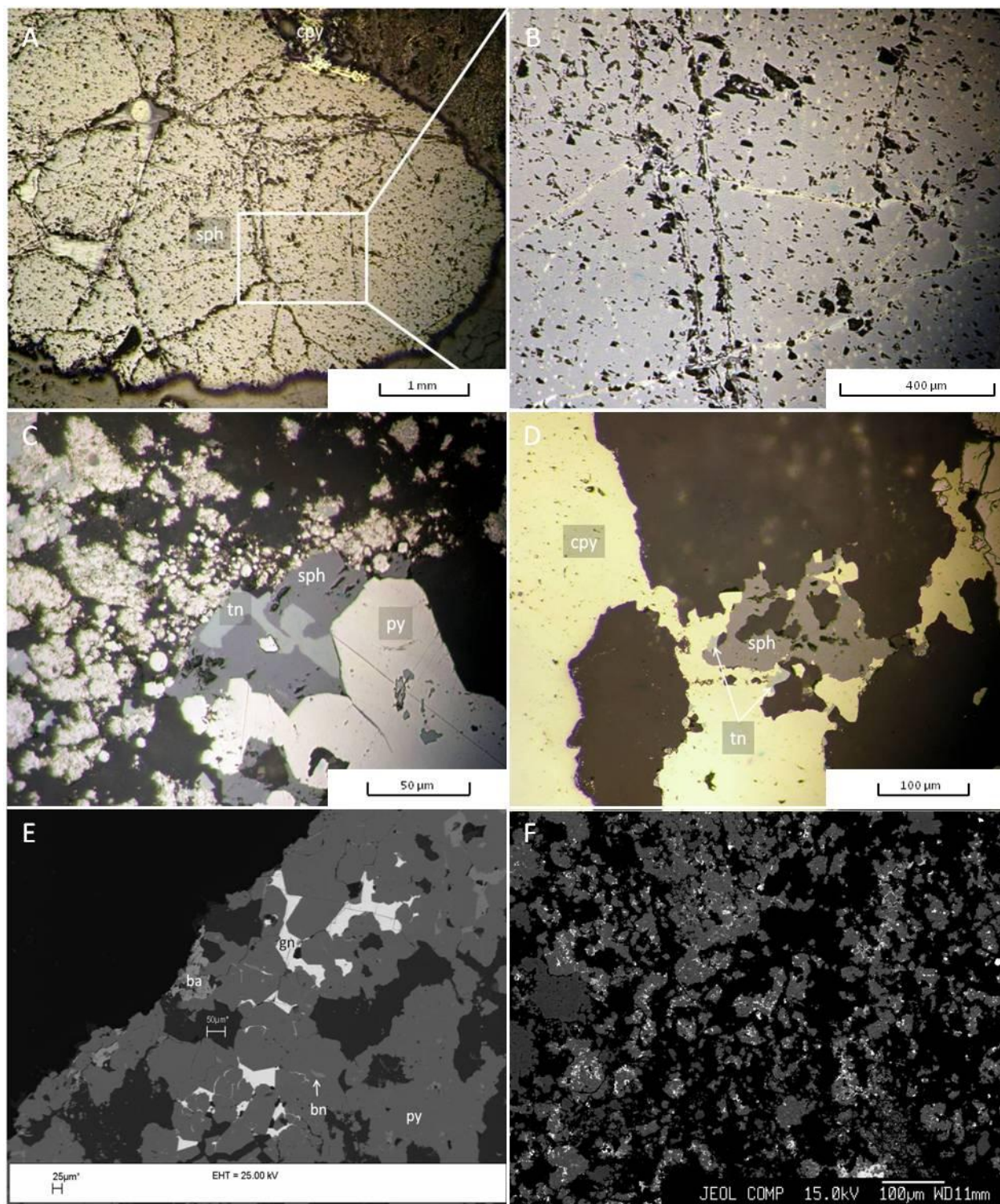


Plate 9: Lead and Zinc Mineralization

A and B) Optical photomicrographs of sphalerite grain showing chalcopyrite disease from USZ; C) Optical photomicrograph of sphalerite intergrown with tennantite adjacent to pyrite II from USZ; D) Optical photomicrographs of sphalerite and minor tennantite adjacent to chalcopyrite from USZ; E) SEM-BSE and reflected light images of galena and bornite filling gaps between pyrite II grains from USZ; F) EMPA-BSE image of pyrite grains surrounded by quartz with abundant galena inclusions from USZ.

3.2.5. Barium and Phosphate Minerals

Barium mineralization occurs throughout the entire Black Butte ore body. It is especially prevalent in the USZ where it occurs as feathered cm-scale barite crystals (figure 6). Barite can also be seen on a microscopic scale as distinct crystals which occur nearly everywhere there is copper mineralization.

Barium can also be seen in the structure of some feldspar grains at Black Butte. Celsian, pure barium feldspar, has been noted as well as hyalophane, i.e., K-feldspar which contains up to 35% ionic replacement of barium for potassium. Although a complete solid solution series between K-feldspar and celsian occurs at temperatures above 700°C (Essene et al., 2005), at lower diagenetic temperatures there is a miscibility gap (gray shaded area on figure 8) which is clearly seen to occur at Black Butte. Given the rarity of Ba-feldspar in nature, the high barite content at Black Butte, and the fine-grained nature of the hyalophane and celsian crystals that were identified by SEM, it is likely that the Ba-rich feldspars formed in-place, during the Stage I hydrothermal event, and were not detrital grains swept into the Belt Basin from erosion of upland areas.

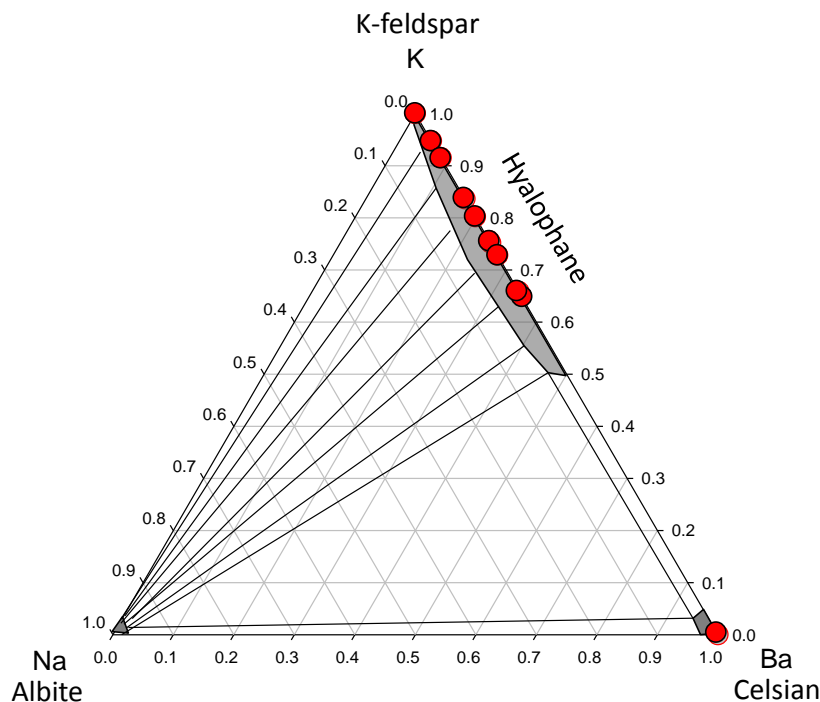


Figure 8: Composition of Feldspars from Black Butte
 Plotted on a ternary Na-K-Ba diagram, red circles are analyses from Black Butte (Appendix B). Shaded region shows the approximate range of hyalophane solid solution under diagenetic ($T < 200^{\circ}\text{C}$) conditions (from Essene et al., 2005).

Apatite ($\text{Ca}_5(\text{PO}_4)_3(\text{OH},\text{F},\text{Cl},)$) is a common gangue mineral at Black Butte, especially in the LSZ. Based on drill core assay results, the apatite tends to be concentrated into discrete zones of limited vertical extent within the greater accumulation of pyrite and other sulfide minerals. In thin section, the apatite crystals are fine grained, sometimes forming botryoidal aggregates that are vaguely similar in shape and size to some of the micro-pyrite aggregates. This being the case, it is possible that pyrite replaced apatite in some cases. One of the most apatite-rich specimens observed in this thesis was closely associated with fine-grained intergrowths of alloclasite and marcasite/pyrite (Plate 5C, 5D) as well as some of the largest siegenite crystals found in this study (visible without a hand lens).

3.3. Assay Data

Tintina Resources provided the author with a complete table of assay data for ore intercepts encountered during the 2010-2011 drilling program. These data include concentrations for 35 elements at specific depth ranges throughout the entire ore body including the USZ and LSZ in both the Johnny Lee and Lowry areas. In this thesis, the assay database has been used to create a series of element cross-plots that can be used to infer mineralogy based upon stoichiometric relationships between selected elements.

Figure 9 shows the correlations between Fe and S, and between Cu and Fe. The red line in Figure 9A corresponds to the trend expected for pure pyrite (or marcasite), whereas the red line in Figure 9B corresponds to chalcopyrite. These diagrams confirm the visual observation that pyrite and marcasite are by far the most abundant sulfide minerals at Black Butte. The fact that Fe plots slightly above the pyrite line suggests the presence of minor amounts of Fe in non-sulfide minerals, such as ferroan dolomite, chlorite, or biotite. Although some samples are quite Cu-rich (e.g. > 50,000 mg/kg, or > 5%), most of the samples contain more pyrite than chalcopyrite and quite a few contain high pyrite and negligible chalcopyrite.

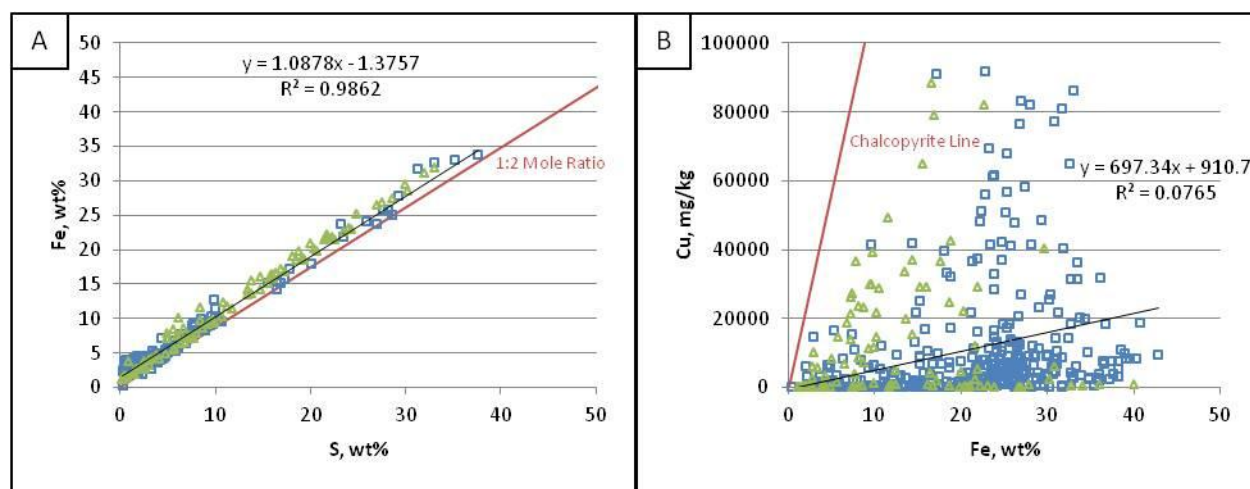


Figure 9: Pyrite and Chalcopyrite Plots
 Blue squares indicate USZ assay value, green triangles indicate LSZ value.

Figure 10 shows the interrelationships between Ni, Co, Cu, and As. The plots on the left (A,C) are on a logarithmic scale to show better trends at low concentrations, whereas the plots on the right have linear axes.

Figures 10A and 10B show that the sum of (cobalt + nickel), when plotted against arsenic, correlates exceedingly well ($R^2 = 0.97$). The heavily clustered samples at and below 100 mg/kg are near the detection limit. Perhaps what is most interesting, as shown in Figure 10B, is that the stoichiometric ratio of (Co+Ni)/As is very close to 1:1, which infers that the main form of Co and Ni at Black Butte is an As-bearing mineral, such as cobaltite (Co,Ni)AsS. Although previous workers (Zieg et al., 1991; Himes and Petersen, 1990) suggested that cobaltite was the most likely form of Co and Ni at Black Butte, the minerals glaucodot and alloclasite have the same general chemical formula, differing only in their symmetry and internal structure. As discussed below, textural evidence found in this thesis suggests that alloclasite is more important than cobaltite at Black Butte. Either way, the predominance of a Co-Ni *sulfarsenide* mineral suggested by the assay data is in contrast to the abundance of siegenite (a Co-Ni *sulfide* mineral) observed in hand sample, polished section, SEM-EDS, and EMPA analysis. If siegenite were the main form of Co and Ni at Black Butte, then the correlation between (Co+Ni) and As would be expected to be poor. This apparent contradiction is an important observation with respect to the genesis of the deposit, and is discussed further in Section 4.1.

Figure 10C shows a general trend of cobalt mineralization accompanying copper mineralization at a ratio of 1:10. This plot shows that enrichment of the two metals coincides spatially, which can be readily observed at Black Butte; every instance of siegenite and cobaltite has been closely associated with copper mineralization. However, although there is a *general*

spatial association between Co and Cu, figure 10D demonstrates that there is no *stoichiometric* correlation between cobalt/nickel mineralization and copper. This is consistent with the absence of any Cu-rich Co-Ni minerals (e.g., carrollite, CuCo_2S_4) at Black Butte.

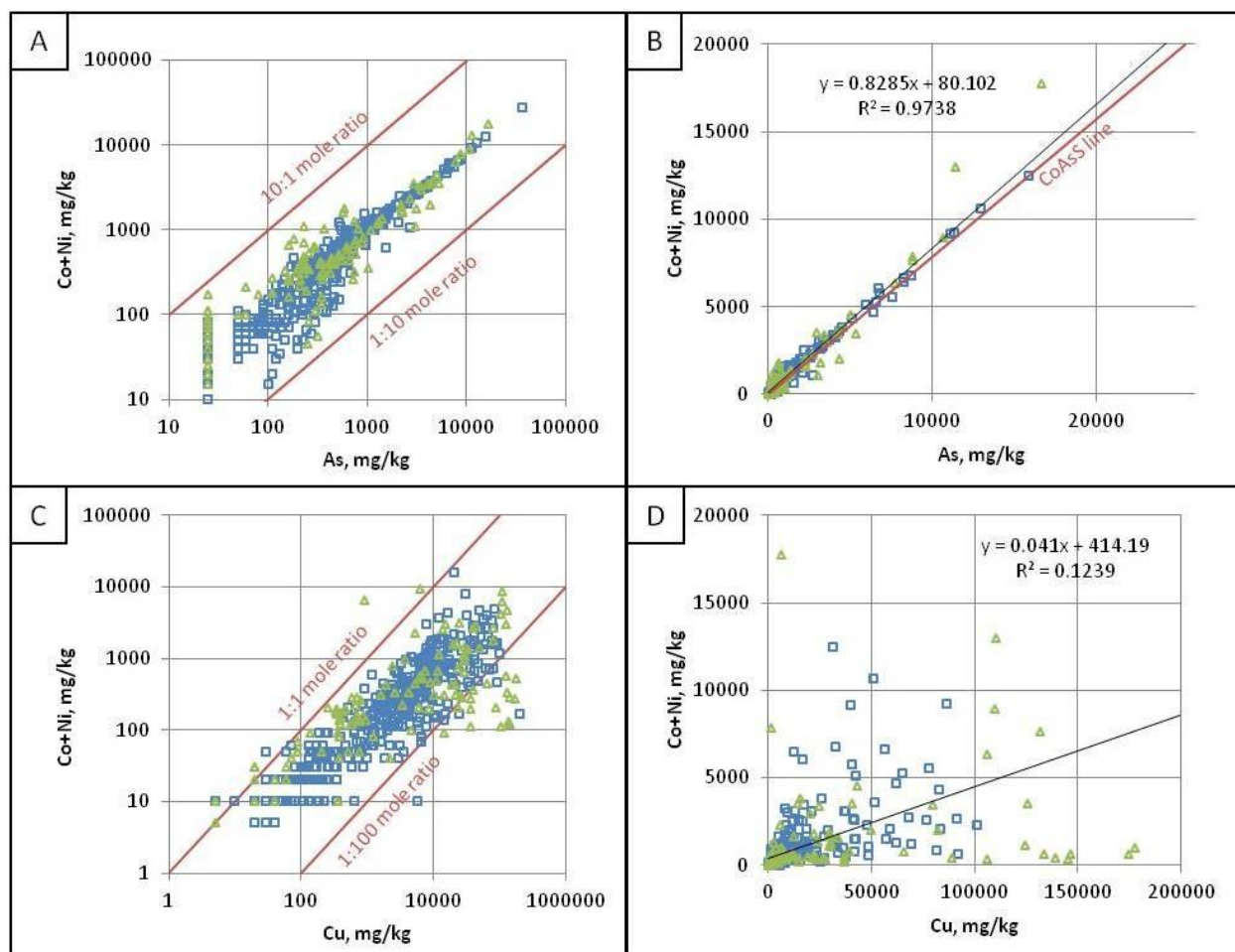


Figure 10: Cobalt Assay Relationships
Blue squares indicate USZ assay value, green triangles indicate LSZ value.

Silver, the third most important economic metal at Black Butte (Table 1), occurs in elevated concentrations throughout the deposit, but is more enriched in the USZ. No discrete silver minerals have been observed in this study, nor in previous mineralogical investigations of Black Butte. Silver is a common impurity within the crystal lattice of galena, occasionally to such an extent that galena is mined as silver ore (mindat.org). Figure 11A shows that silver and lead are correlated ($R^2 = 0.57$) at Black Butte, which suggests that perhaps the majority of silver mineralization occurs as impurities within the galena. Of the two EMPA analyses that were performed on galena grains at Black Butte, one did contain silver in concentrations above the detection limit (0.01 atomic percent), so it is possible. Contrarily, figures 11B and 11C demonstrate that silver has no correlation with copper or arsenic. This suggests that the primary Ag-bearing phase is neither chalcopyrite nor tennantite. Interestingly, silver was detected in EMPA analyses in both chalcopyrite and tennantite at very low concentrations (0.01 atomic percent or less), indicating that while not a primary sink, silver is contained within copper minerals. Finally, figure 11D shows that silver and gold have no stoichiometric correlation. This is unusual given that these two metals often are associated together, as in the mineral electrum. The lack of association of these metals could also be caused by their spatial separation in the deposit; silver is found primarily in the USZ whereas gold is hosted exclusively in the LSZ. This can be clearly seen in figure 11D; the Ag-rich ore from the USZ has little Au and plots along the Y-axis, and the Au-rich ore from the LSZ has little Ag and plots along the X-axis. If only the LSZ samples are considered, there is a possible relation between Ag and Au, with a slope close to 10:1 (wt %).

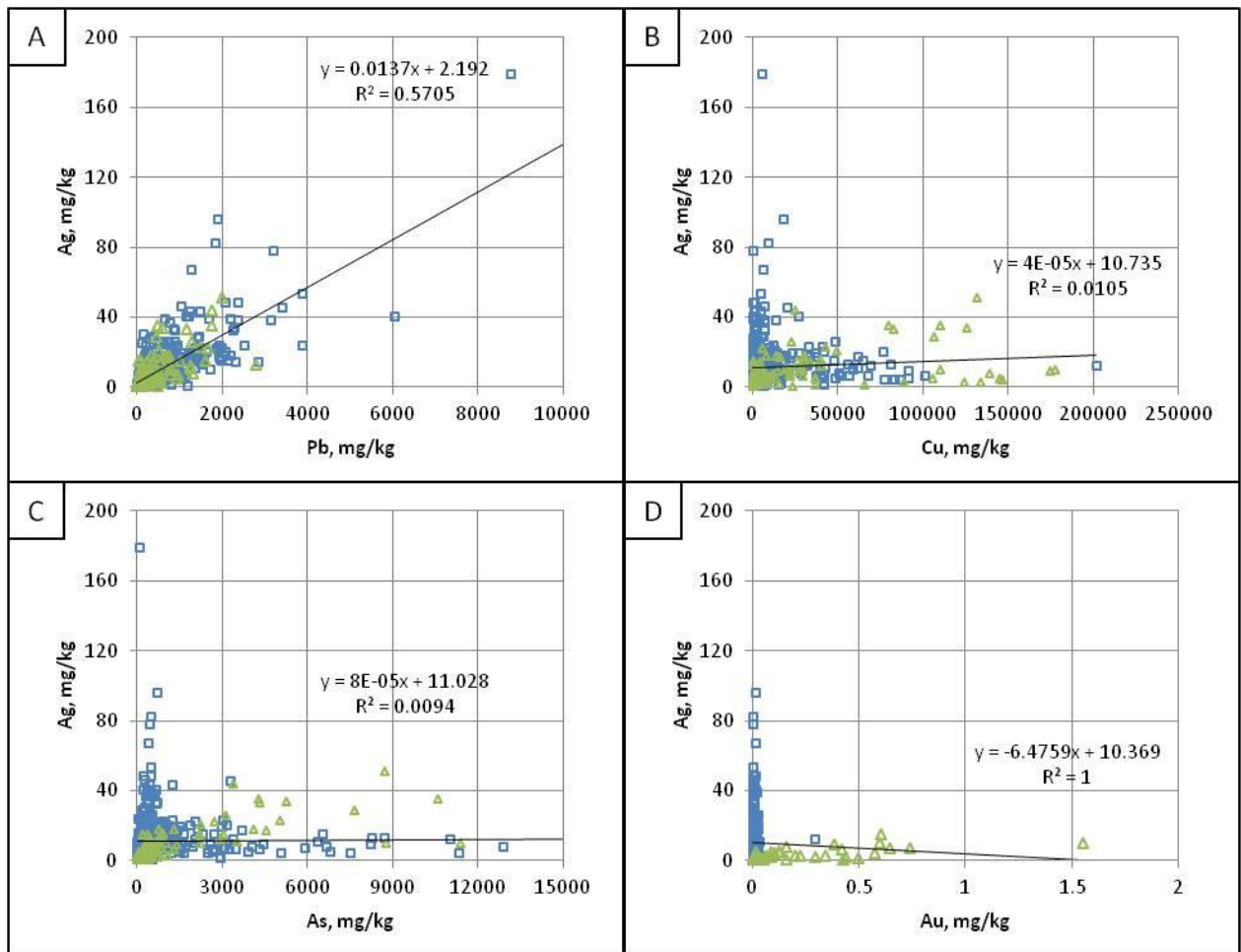


Figure 11: Silver Mineralization Plots
Blue squares indicate USZ assay value, green triangles indicate LSZ value.

Figure 12A demonstrates that most of the P-rich assay samples plot close to the stoichiometric P:Ca ratio that corresponds to apatite, $\text{Ca}_5(\text{PO}_4)_3(\text{OH})$. As discussed above, apatite is locally an abundant mineral at Black Butte. In the LSZ, a significant portion of the calcium is hosted within apatite, whereas in the USZ phosphorous is nearly absent and calcium is contained primarily within the carbonates. Figure 12B shows a correlation between gold and phosphorous, which suggests that gold and apatite are spatially associated within the LSZ, but not stoichiometrically related.

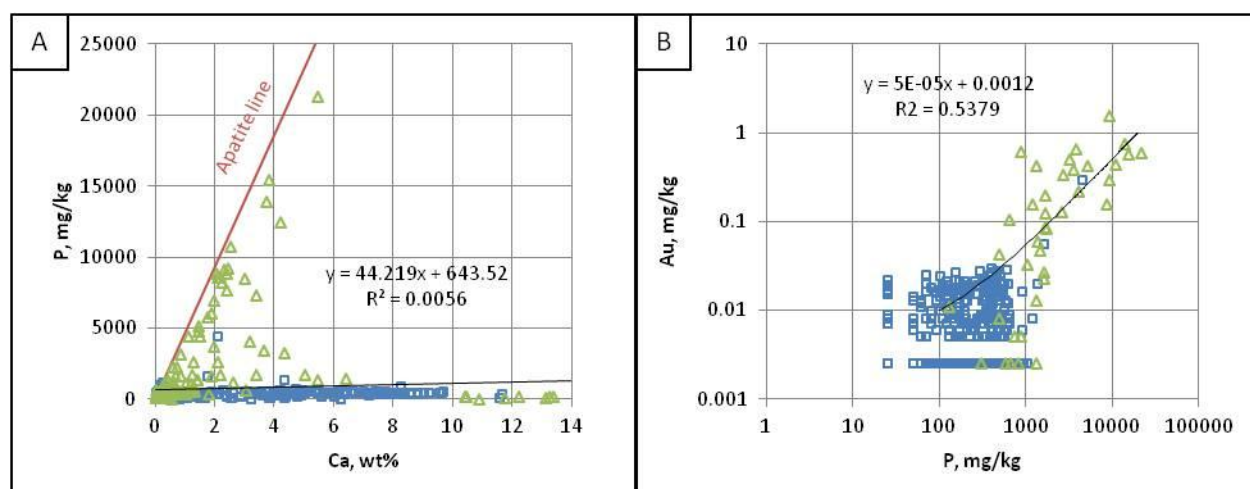


Figure 12: Phosphorous Plots
Blue squares indicate USZ assay value, green triangles indicate LSZ value.

3.4. Carbon Isotopes

In northern Australia it has been demonstrated that several of the large SEDEX ore bodies, including HYC and Lady Loretta, have lithogeochemical halos surrounding them which can be used as indicators of the presence of economic mineralization (Large et al., 2001, and references therein). These deposits have elevated levels of Fe, Mn, Zn, Pb, and Ti in the sedimentary rocks which surround them. Further, Large et al. (2001) showed that McArthur River has an extensive isotopic halo in which the host dolomite rock is enriched in ^{18}O and depleted in ^{13}C in a stratigraphic zone that extends > 10 km to the south of the ore body.

Because of the similarities that Black Butte shares with the McArthur River ore body (similar age and host rocks), it was postulated that perhaps an isotopic halo in $\delta^{13}\text{C}$ or $\delta^{18}\text{O}$ of carbonate in the Newland Formation would exist at Black Butte. If true, this might serve as a potential exploration tool to find new ore bodies in the district. Isotopic results for carbonate samples taken from drill hole SC11-021 are shown in Table 9 and Figure 13. Samples collected between depths of 120 and 160m were from the USZ itself, and contained insufficient carbonate minerals for an isotopic analysis. The lack of carbonate is explained by the abundance of pyrite and other sulfide minerals, coupled with the high quartz and barite content of the USZ.

The plots in Figure 13 show no clear trend in $\delta^{13}\text{C}$ or $\delta^{18}\text{O}$ of carbonate minerals in the Newland Formation approaching the USZ sulfide horizon from either the top or the bottom. In the future, it might be worthwhile to examine the carbonate isotopes in drill holes located within the same USZ stratigraphic interval, but well outside of the Johnny Lee ore resource.

Table 9: Carbonate Isotope Results

Sample	Depth (m)	$\delta^{13}\text{C}$, ‰ (VPDB)	$\delta^{18}\text{O}$, ‰ (VPDB)	$\delta^{18}\text{O}$, ‰ (VSMOW)
1	76.8	No analysis*	No analysis*	No analysis*
2	83.5	-1.6	-6.0	24.7
3	88.1	-1.0	-6.5	24.2
4	93.6	-0.5	-9.5	21.1
5	99.2	-0.1	-5.7	25.0
6	104.5	-0.4	-6.4	24.3
7	110.0	-0.6	-7.8	22.9
8	115.8	-0.4	-8.7	22.0
9	120.7-ore	No analysis*	No analysis*	No analysis*
10	129.2-ore	No analysis*	No analysis*	No analysis*
11	139.1-ore	No analysis*	No analysis*	No analysis*
12	160.9-ore	No analysis*	No analysis*	No analysis*
13	166.7	-0.3	-7.3	23.4
14	171.8	-0.4	-7.3	23.4
15	177.2	-0.2	-6.9	23.8
16	183.5	-0.1	-6.7	24.0
17	188.1	0.0	-7.2	23.5

*These samples contained insufficient carbonate minerals for a stable isotope analysis.

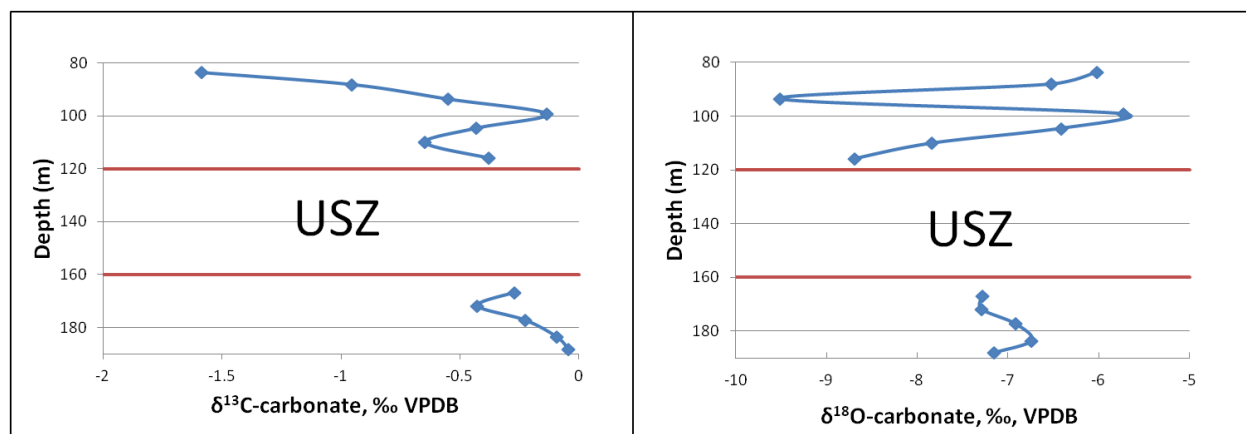


Figure 13: Isotopic Composition of Carbonate as a Function of Depth

It is interesting to note that the carbon isotopic composition is very close to 0‰, which is the expected value for carbonate minerals sourced from seawater in the Mid-Proterozoic (Chu et al., 2007). This could be taken as evidence that the Belt Ocean in the vicinity of the Helena Embayment was marine, not lacustrine. Freshwater limestones usually have $\delta^{13}\text{C}$ values that are much lighter (more negative). The $\delta^{18}\text{O}$ plot, shown on the right, has significant variation with depth and exhibits no particular trend, but has an average of approximately -7‰ VPDB. This is also consistent with a marine origin for the Newland Fm., because Proterozoic carbonate values worldwide range from -10‰ to -7‰ VPDB (Ray et al., 2003). Some of the variations with depth for both $\delta^{13}\text{C}$ and $\delta^{18}\text{O}$ may reflect variable amounts of isotopic exchange between carbonate minerals in the Newland Fm. with younger groundwaters.

4. Discussion

4.1. Mineralization at Black Butte

The mineral chemistry of the sulfide horizons at Black Butte suggest at least two periods of mineralization for this deposit. There are multiple lines of mineralogical and geochemical evidence supporting this theory which will be discussed further in the following sections. Simply stated, Stage I is interpreted to represent syngenetic mineralization formed at the same time as deposition of the enclosing sediments, whereas Stage II is interpreted as being diagenetic, and formed after deposition and burial of the Newland Fm. Below is a paragenesis diagram which outlines the relative timing and abundances of important minerals within the deposit (Figure 14). Although there is evidence suggesting that the geochemical environments of the two sulfide horizons during mineralization were not identical, Stage II mineralization is assumed to have affected the entire ore body when active, but with varying degrees of influence.

Mineral	Stage I	Stage II
Pyrite I		
Marcasite		
Chalcopyrite		
Pyrite II		
Tennantite		
Siegenite		
Alloclasite		
Bismuthinite		
Galena		
Sphalerite		
Bornite		
Chalcocite		
Quartz		
Dolomite		
Barite		
Ba-Feldspar		
Apatite		

Figure 14: Paragenesis Diagram

Note that the size of the shape determines the relative abundance of each mineral with respect to each stage of mineralization.

4.1.1. Cobalt/Nickel Paragenesis

This study has found that nearly all cobalt and nickel minerals at Black Butte visible in hand sample or under a petrographic microscope are siegenite $(\text{Co},\text{Ni})_3\text{S}_4$. However, the stoichiometric relation between $(\text{Co} + \text{Ni})$ and As displayed in the whole-rock assay data strongly suggests mineralization in the form of a sulfarsenide with the stoichiometry $(\text{Co}+\text{Ni})\text{AsS}$. Although cobaltite is the most familiar ore mineral with this stoichiometry, glaucodot and alloclasite also have the formula CoAsS . Only trace amounts of very fine-grained

Co-Ni sulfarsenide minerals have been found in this study using SEM and EMPA analysis, and these were only found in samples from the LSZ.

The apparent contradiction between the dominance of siegenite and the tight correlation between Co+Ni and As is explained with two stages of mineralization. The early, syngenetic Co-Ni minerals in Stage I were likely extremely small ($< 1 \mu\text{m}$, possibly much smaller) nickel-rich alloclasite inclusions hosted within “impure” pyrite and marcasite. This pyrite can still be observed at Black Butte and has been labeled pyrite I (Plate 2). Stage II mineralization introduced more copper to the system, but did not add more cobalt or nickel. Instead, the early sulfarsenide inclusions were reworked and reprecipitated as at least two new distinct minerals. Arsenic, along with copper which had been either introduced during Stage II or removed from existing copper minerals, formed tennantite. The cobalt and nickel precipitated as siegenite. The textural relationships observed (Plates 7 and 8) show that siegenite is nearly always found associated with tennantite and pure euhedral pyrite II.

If the above argument is correct, then it must follow that Stage II mineralization could not have moved the Co, Ni and As present in Stage I pyrite very far. If it did, then the very tight relationship between (Co + Ni) and As in bulk-rock assays would no longer be seen. Instead, it appears that the mobility of Co, Ni and As must have been fairly low during Stage II. This relationship is evidenced by the close association of siegenite and tennantite which is seen throughout Black Butte.

4.1.2. Evidence for Alloclasite

Both the SEM-EDS at Montana Tech and the EMPA at WSU identified tiny inclusions of a Co-Ni sulfarsenide mineral with the general formula $(\text{Co}+\text{Ni}+\text{Fe})\text{AsS}$. However, there are three possible minerals with this stoichiometry: cobaltite, glaucodot, and alloclasite. Judging

from images available on the internet (Mindat, 2012), cobaltite and glaucodot tend to form individual euhedral crystals, whereas alloclasite often forms rosettes of fine-grained crystal aggregates. The latter texture was observed from the Lower Sulfide Zone, where the Co-Ni sulfarsenide minerals are finely intergrown with an unidentified FeS_2 phase (either pyrite or marcasite). The distinctive texture of $(\text{Co}+\text{Ni}+\text{Fe})\text{AsS}$ growing on two sides of euhedral marcasite crystals but not on the other two sides is also interpreted as favoring the idea that alloclasite is the dominant Co-Ni sulfarsenide phase. The following diagram (Figure 15, from Yang and Downs, 2008) summarizes the crystal structure of marcasite, alloclasite, and glaucodot. As shown by the middle panel, it is possible for alloclasite to grow epitaxially on two faces of a marcasite crystal, but not on the other two. Glaucodot, on the other hand, cannot grow epitaxially on any crystal face of marcasite, nor can cobaltite. Finally, since low temperatures usually favor precipitation of polymorphs of lower symmetry (Nesse, 2012), this again favors the sulfarsenide phase being alloclasite (monoclinic) as opposed to cobaltite (isometric) or glaucodot (orthorhombic). A definitive identification would require XRD analysis, which was not possible in this study given the low abundance and minute size of the sulfarsenide minerals.

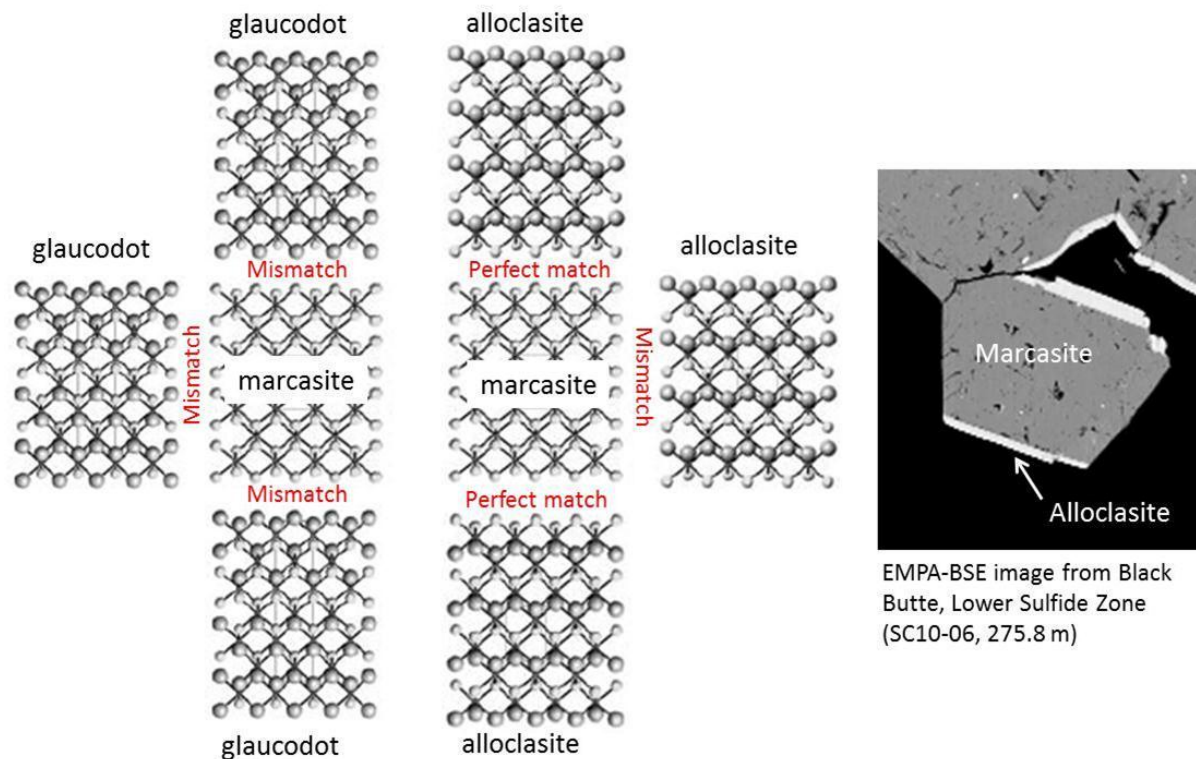


Figure 15: Crystal structure comparison of marcasite, glaucodot, and alloclasite
 Crystal models from Yang and Downs, 2008. Large, medium, and small spheres represent As, S, and Co-Ni-Fe atoms, respectively.

4.2. Physical and chemical conditions of ore formation

As discussed earlier, Black Butte was formed during two distinct periods of mineralization. The first period, Stage I, brought in the majority of the metallic elements, and Stage II reworked the existing metals while introducing additional copper and minor amounts of other metals.

4.2.1. Stage I Mineralization

Stage I mineralization occurred during deposition of the Newland Formation in the Helena Embayment. During the sedimentation of the Helena Embayment, after the formation of the synsedimentary buttress fault(s), ore fluids moved up the fault forming a brine pool in the topographically low area adjacent to the fault, developing the SEDEX type deposit present today.

There were at least three periods of heightened fluid movement corresponding to the three sulfide horizons seen at Black Butte, with the first and third events providing enough fluid to form laterally continuous brine pools. Between periods of hydrothermal activity, sediment deposition continued in the basin, laying down the shale and carbonates between the sulfide horizons.

The brine pools from which the sulfide horizons precipitated were probably low temperature ($<100^{\circ}\text{C}$), for the following reasons. First, if the circular pyrite structures described in the previous chapter are indeed vent fauna, then such organisms could not have survived at temperatures much higher than 100°C , the upper limit for thermophiles. Second, S-isotope data for pyrite in the Newland Fm., summarized by previous workers (Lyons et al., 2000), suggest that much if not most of the pyrite formed from bacterial reduction of sulfate. Sulfate-reducing bacteria are mesophiles, meaning they could not exist at temperatures much above 50°C . Finally, examination of modern-day brine pools formed by SEDEX-type ore fluids, such as occur at the bottom of the Red Sea (Degens and Ross, 1969), indicates that such brine pools have temperatures $< 60^{\circ}\text{C}$. Some mineralogical constraints on the pH of the brine pool exist. For example, the presence of dolomite and authigenic, barium-rich K-feldspar suggests a near-neutral pH. On the other hand, the abundance of marcasite in the primary ore could be interpreted as evidence of periodic excursions to lower pH. Marcasite, believed to be remnant from initial mineralization, will only grow as a primary phase in an environment with a pH of less than 5, a temperature less than 240°C , and in the presence of H_2S (Murowchick, 1984, and others). One way to lower pH would be if some H_2S in the brine pool was oxidized to sulfuric acid. This suggests that there may have been periodic mixing of the water column leading to temporary, spatially-limited oxidizing conditions which would lower the pH sufficiently to

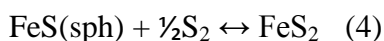
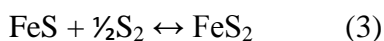
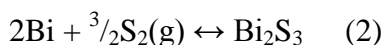
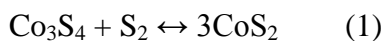
promote the formation of marcasite. Periodic mixing of the water column is supported by the presence of turbidites and small conglomerate layers (debris flows?) seen in the laminated shale throughout the ore body. Barite (BaSO_4), seen throughout the USZ, provides further evidence supporting limited oxidizing conditions within the Stage I brine pool (Himes and Petersen, 1990).

While the previous paragraph focused on the environment of the brine pool that formed Stage I mineralization, there are few clues as to the temperature and chemistry of the hypogene ore-forming fluids *themselves*, i.e., the fluids that vented into the brine pools. They must have had a density greater than cold seawater, and they must have been capable of transporting the various ore constituents that accumulated in the massive sulfide piles (i.e., Fe, Cu, Co, Ni, As). In the case of the USZ, a predominance of quartz and relative scarcity of dolomite suggests that the ore fluids were hot enough to transport a lot of silica and very little carbonate. In modern hot spring environments (e.g., Yellowstone Park), high-temperature ($T > 200^\circ\text{C}$) geothermal systems tend to precipitate silica on the surface (as at upper or lower Geyser Basins), whereas lower-temperature systems ($T < 200^\circ\text{C}$) deposit mainly travertine (as at Mammoth Springs) (Fournier, 1989). The reason for this difference is the fact that quartz has prograde solubility (it becomes more soluble as temperature increases) whereas the solubility of calcite and dolomite is retrograde (e.g., Holland and Malinen, 1979). It is also possible, as suggested by Graham et al. (2012), that silica was introduced by hot hydrothermal fluids *after* burial of the Newland Formation, and replaced pre-existing dolomite. However, if this were the case, then one might expect to see more evidence of silicification, such as quartz veining or stockworks in the footwall of the deposit. In future work, it would be very interesting to look for possible feeder zones to the stratiform mineralization at Black Butte.

4.2.2. Stage II Mineralization

Stage II mineralization, possibly initiated by the introduction of thermal energy into the system by a magmatic injection forming a sill, occurred after deposition and burial of the Newland Formation. A hydrothermal fluid permeated through the pre-existing ore bodies and, along with introducing an additional volume of copper, reworked the existing mineralization.

The second stage of mineralization contained several ore minerals that are sensitive indicators of temperature and S_2 -activity. Figure 16 shows the activity of $S_2(g)$ plotted as a function of temperature for several reactions involving hydrothermal sulfide minerals. In terms of constraining the T- a_{S_2} conditions of Stage II mineralization, the following reactions are most useful:



Note that the thermodynamic data for reactions (1) and (2) are considered excellent (Barton and Skinner, 1979), whereas that for (3) is considered poor. However, reaction (3) is not relevant to Black Butte, since no pyrrhotite has been found in the deposit. In the presence of sphalerite and pyrite, reaction (4) can be used instead of reaction (3). Here, it is the FeS component in sphalerite that reacts with S_2 to form pyrite. There are two sets of thermodynamic data that can be used to model the Fe-content of sphalerite: Scott and Barnes (1971) and Toulmin and Barton (FeS₂, 1964) + Richardson and Jeffes (FeS, 1952). Also, it is important when applying this a_{S_2} -indicator to make sure that the Fe-content of sphalerite is homogeneous (no internal zoning) and has not been affected by a later reaction, such as chalcopyrite disease (i.e., replacement of FeS in

sphalerite by CuFeS_2). Although rare, some sphalerite was found in Stage II mineral assemblage that was free of chalcopyrite disease. EDS analyses of 10 different grains gave an average composition of $\text{Zn}_{0.098}\text{Fe}_{0.019}\text{S}$, with X_{FeS} ranging from 0.0033 to 0.0330. Putting this composition into the equations of Barton and Skinner (1979) for the two thermodynamic data sets gives the two curves shown in Figure 16 that are shaded brown.

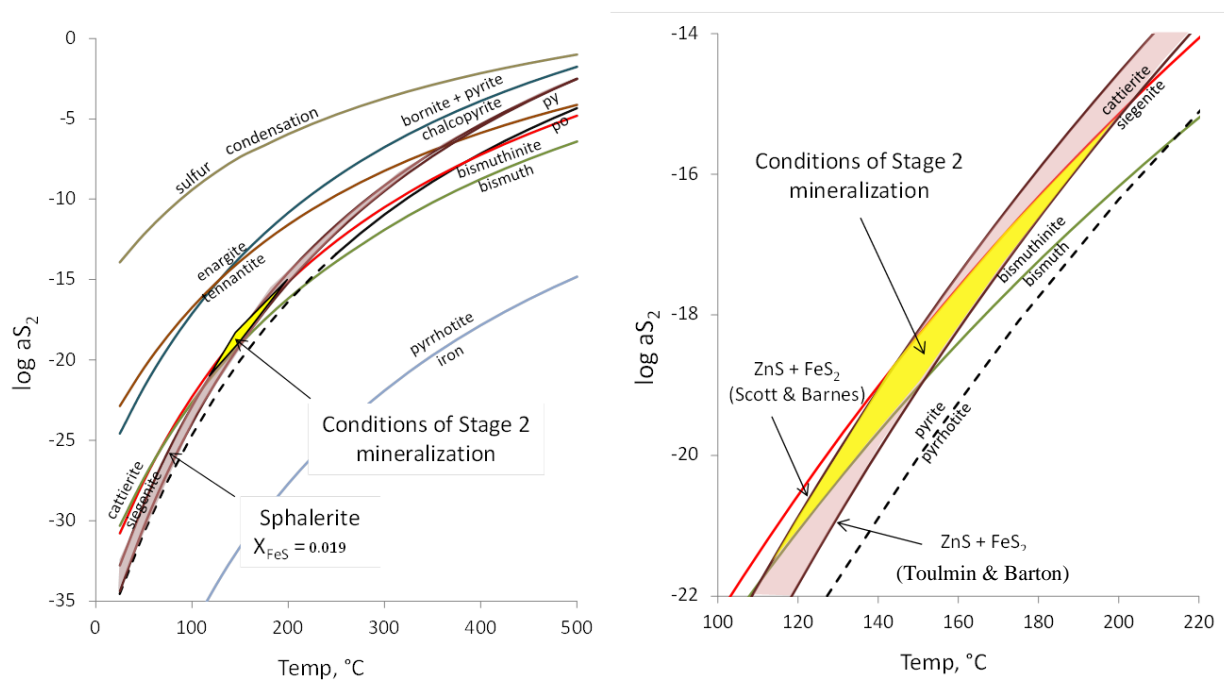


Figure 16: a_{S_2} -Temperature Diagram for Minerals Found at Black Butte

The yellow area corresponds to the conditions of formation of Stage 2 (note expanded scale of right panel). The light brown shading shows the range in stability for sphalerite ($X_{\text{FeS}} = 0.019$) in equilibrium with pyrite based on different thermodynamic data.

The assemblages bismuthinite + siegenite and pyrite + sphalerite place tight controls on the activity of $\text{S}_2(\text{g})$ ($a_{\text{S}_2} = 10^{-21}$ to 10^{-17}) and temperature ($T = 110^{\circ}\text{C}$ to 200°C) during Stage II mineralization, as shown in Figure 16 (yellow area). Solid solution of Ni into siegenite will expand its stability field to higher values of a_{S_2} , but the shift is predicted to be minor given the scale of the y-axis. Also, it is likely that any catterite (CoS_2) that might form at higher a_{S_2} would also be impure (i.e., Ni-rich), which would counteract the effect of impure siegenite. A

moderate drop in aS_2 would cause the ore fluids to enter the pyrrhotite field, a mineral that has not been identified yet in thin section. Other minerals in the ore, such as tennantite and chalcopyrite, are also stable in the yellow area.

The uncommon occurrence of bornite, chalcocite, and enargite in some samples suggests a local deviation to much higher aS_2 and/or a drop in temperature. The bornite and chalcocite observed in this study were usually coarse grained, filling pore space between pre-existing minerals, and were clearly late in the paragenesis.

4.3. Source of metals

The origin of the distinct metal associations at Black Butte is as important as the chemical environment in which they were deposited to the understanding of the origin of this deposit. Schieber (1991) suggests that the lack of lead and zinc mineralization at Black Butte is due to an insufficient thickness of clastic sediments below the deposit to have been scavenged for these metals. This argument is weakened, however, by the presence of the Soap Gulch Deposit near Melrose, MT which is a Pb-Zn SEDEX type deposit that is hosted in the Newland Formation. Also, during the ongoing drilling performed by Tintina Resources, significant Pb and Zn intercepts (ore grade but not mineable) have been identified at Black Butte, specifically in the southern and western parts of the district (G.A. Zieg, personal communication, April, 2012).

A second possible explanation for the lack of economic Pb and Zn mineralization has to do with the geochemical conditions of the ore forming fluid which provided the majority of the metallic mineralization at Black Butte. The ore fluid which formed the Stage I brine pool was preferentially enriched in Cu, Co, Ni, and Ag, while containing only minor amounts of Pb, Zn, and Au. How did an ore fluid with this metal chemistry evolve? Rose and Bianchi-Mosquera (1993) conducted a series of experiments to test for the relative solubility of different metals

under pH and redox conditions believed to be important in the generation of red-bed copper deposits. These authors illustrated that changes in the temperature, salinity, and redox state (i.e. Eh) within a typical red-bed sandstone can change the relative mobility of Cu and other metals in an ore-forming fluid where metal concentrations are limited by adsorption onto goethite or hematite. For example, at 25°C and in oxidized (air saturated) conditions, a saline brine with a pH near 7 will transport Zn, Co, and Ni, but not Pb or Cu (Figure 17A). In contrast, the same solution at 50°C and pH 7 but with redox buffered to moderately reducing conditions (Fe^{2+} / goethite) will transport mainly Cu, with lesser amounts of Ni and Co, and virtually no Pb or Zn. As pointed out by Rose and Bianchi-Mosquera (1993), the main reason for the drastic shift in position of copper between Figures 17A and B has to do with the redox state of copper. In air-saturated conditions, Cu(II) is the stable valence state, Cu^{2+} is the dominant aqueous species, and Cu^{2+} adsorbs strongly onto Fe-oxides. However, at lower redox state and in the presence of high NaCl concentrations, Cu(I) chloride complexes become the dominant form of dissolved Cu, and these species do not adsorb strongly onto Fe-oxides. Thus, a hot brine ($T < 150^\circ\text{C}$) circulating through a red sandstone at pH 7 and moderately reducing Eh will transport Fe (as Fe^{2+}) $>$ Cu $>$ $(\text{Ni} + \text{Co}) >$ $(\text{Zn} + \text{Pb})$, which are the ratios seen within the Black Butte deposit. Because Fe-oxides are also effective scavengers of dissolved arsenate and phosphate (Drever, 1997), partial dissolution of the Fe-oxides in the red-bed could provide a source of soluble As and P, two elements that are also enriched at Black Butte.

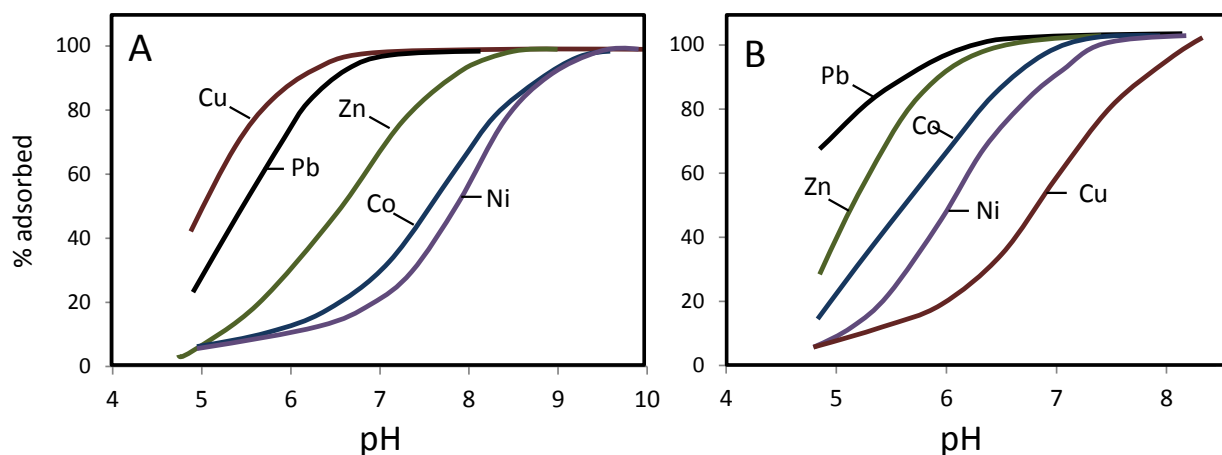


Figure 17: Adsorption of Cu, Pb, Zn, Co, and Ni onto Goethite as a Function of pH
A) at 25°C, 1 molal NaCl, in presence of air; B) at 50°C, 1 molal NaCl, with Eh buffered by Fe²⁺/goethite.
Modified from Rose and Bianchi-Mosquera (1993).

Interestingly, Rose (1989) noted that while the ratios of Cu/Ag/Zn/Co/Ni/Pb are usually within one order of magnitude in sediments world-wide, these ratios can vary many orders of magnitude within the spectrum of sediment-hosted ore bodies. Rose and Bianchi-Mosquera (1993) concluded that the metal ratios of the source beds are probably less important than discriminatory processes such as sorption/desorption that mobilize some elements but not others from the source bed into the ore-forming fluid.

4.4. Comparison of Black Butte to other ore-deposit models

Black Butte does not fit into any classically defined ore body type, but rather exhibits geochemical characteristics of both “sedimentary exhalative” (SEDEX) and “red-bed copper” deposits. This section will begin with a brief overview of these two types of deposits and then will discuss in more detail to Black Butte.

4.4.1. SEDEX Deposits

According to the review of Leach et al. (2005), sedimentary exhalative (SEDEX) deposits share the following general characteristics: 1) they occur as tabular Pb-Zn (\pm Ag, Cu, Ba) ore

bodies containing laminated ore minerals (pyrite, sphalerite, galena \pm chalcopyrite, pyrrhotite, barite) parallel to bedding; 2) they are hosted by marine sediments, including black (carbon-rich) shale, siltstone, and carbonates; 3) associated igneous rocks (volcanic or intrusive) are usually absent or volumetrically minor; and 4) they typically form in active rift environments. Examples of world class SEDEX deposits include Red Dog (Alaska), Howard's Pass (Yukon Territories, Canada), Sullivan (British Columbia, Canada), McArthur River (Australia), and Mt. Isa (Australia). In a classic SEDEX model, saline and metal-rich ore fluids are expelled through fractures in the sediment pile out onto the sea floor where, owing to their high density, they sink to form a "brine pool". The metals slowly precipitate out of this brine pool, forming a pile of fine-grained sulfides, along with silica and other gangue minerals. Notably, some SEDEX deposits (e.g., Red Dog, Howard's Pass) are enriched in apatite (Leach et al., 2005). Some SEDEX deposits contain ore in the footwall "feeder zone", which is inferred to represent the area where hot, ore-bearing fluids passed prior to reaching the sea floor. However, many SEDEX deposits have no obvious alteration assemblage in the footwall, which makes it difficult to locate the fluid conduits which fed the system. Based on the review of Leach et al. (2005), ore fluids that bring metals into the SEDEX environment are thought to be highly saline (up to 20 wt% NaCl_{eq}), with temperatures in the range of 100 to 200°C, possibly higher in some cases.

In the preceding summary, the only characteristic of SEDEX deposits that does NOT fit well with Black Butte is the metal associations. Unlike most SEDEX deposits, Black Butte is rich in Cu, with substantial Co and Ni, and contains sub-economic quantities of Pb and Zn. Otherwise, the following characteristics of SEDEX are well displayed at Black Butte: 1) laminated sulfides parallel to bedding; 2) shale/dolomite host rock; 3) no obvious igneous rocks

associated with ore; 4) structural control by rift-bounding faults (i.e., the buttress fault(s) bounding the Helena Embayment); and 5) barite- and apatite-rich layers.

4.4.2. Red-Bed Copper Deposits

The following summary of red-bed copper deposits (also known as sediment-hosted, stratiform Cu deposits) is taken from the review articles of Gustafson and Williams (1981) and Hitzman et al. (2005).

Red-bed copper deposits account for 23% of global production and reserves of copper. Red-bed copper deposits are characterized by the following: 1) a mineral assemblage that is rich in Cu, often accompanied by important levels of Co and Ag, with lesser amounts of Pb, Zn, and U; 2) presence of thin (<30 m) sulfide-bearing horizons that are contained within and parallel to the surrounding lithological layers; 3) disseminated nature of the ore minerals (as opposed to accumulations of massive sulfide in SEDEX); 4) localization of ore within reduced (usually carbonaceous) sedimentary rocks formed in shallow marine or lacustrine environments; 5) presence of laterally extensive, hematite-rich “red-bed” sediments in the immediate hanging wall or footwall of the orebody; and 6) deposit-scale zonation of metal ratios and ore minerals, often with distinct zones rich in one of the following minerals: native copper, chalcocite, bornite, chalcopyrite. Examples of large red-bed copper deposits include the Kupferschiefer (Germany, Poland), the African Copperbelt (Congo, Zambia), White Pine (Michigan) and the Spar Lake and Rock Creek deposits (Montana). Although several models have been proposed for red-bed copper deposits, most are in agreement that the copper and associated metals were sourced from hot brines migrating through the red bed, and that deposition of copper occurred at the redox boundary near the red bed/reduced sediment interface. Unlike SEDEX deposits, the Cu-rich ore fluids that form a “classic” red-bed Cu deposit do not vent at the sea floor.

Black Butte exhibits some of the characteristics of red-bed copper deposits listed above. First among these is the fact that the deposit shows the characteristic enrichment in Cu, Co and Ag, and relative scarcity of Pb and Zn. Also, the Newland Formation which hosts the ore is a strongly reduced, carbonaceous shale. However, there are no red, continentally-derived sediments above or below the ore-bearing horizons (although there is a red quartzite deeper in the stratigraphic section, as discussed below). The ore at Black Butte consists of massive beds of sulfide (mostly pyrite) that are intimately interbedded with marine sediment. Although there is some zonation in minor metals and gangue (e.g., more barite and Ag in the USZ and more apatite and Au in the LSZ), the main ore minerals of copper (chalcopyrite) and cobalt (siegenite) are dominant throughout the deposit. Bornite and chalcocite are present, but are never more abundant than chalcopyrite (although small spatially constrained zones of bornite enrichment have been noted in the deposit), and elemental copper has not been found at Black Butte.

The preceding discussion suggests that, while Black Butte formed in a typical SEDEX environment, it was mineralized with a red-bed type ore fluid. One possible explanation for this ore fluid chemistry is the presence of a red-bed source rock deeper in the Helena Embayment stratigraphy through which the ore fluid would have passed, providing an environment conducive to red-bed mineralization. Lying on top of the Archean bedrock at the bottom of the basin is the Neihart Quartzite, which is an oxidized sediment (pink to brownish-red in outcrop) that may have acted as a source rock for Cu, Co and Ni. Although 200 m of black shale of the Chamberlain Formation is located between the Neihart and the Newland Formation, it is envisioned that the northern border of the Helena Embayment was cut by many normal faults (i.e., “growth faults”), some of which could have served as conduits to release geo-pressurized ore fluids in the Neihart directly to the Newland-aged Belt Ocean. However, if the hypothesis of

the Neihart being an important source bed for Cu-rich ore fluids is correct, then it logical that some extent of stratiform Cu mineralization should exist at the bottom of the Chamberlain Fm. This type of mineralization has not been found to date, although exploration in the Helena Embayment continues.

5. Conclusions and Recommendations

5.1. Conclusions

- The Black Butte ore body consists of a series of laterally-extensive massive sulfide horizons within the lower Newland Fm. of the Belt Supergroup.
- Mineralization is dominated by pyrite±marcasite and chalcopyrite, with lesser amounts of Co-Ni-Ag mineralization.
- Black Butte had two main stages of mineralization. Stage I was syngenetic, and resulted in laminated massive-sulfide ore dominated by fine-grained pyrite and chalcopyrite. Some Stage I pyrite has an unusual “hoop”-shaped morphology, which has been tentatively interpreted as being biogenic in origin. More commonly, Stage I pyrite consists of framboids or amorphous, porous aggregates of micron-sized crystals.
- Stage I pyrite is impure, with elevated Co-Ni-Cu-As, and locally contains tiny grains of Ni-rich alloclasite and/or cobaltite (both are polymorphs of CoAsS). Alloclasite also occurs as epitaxial overgrowths on two opposing sides of euhedral marcasite grains.
- Stage II was epigenetic, and resulted in the introduction of large amounts of copper, as well as recrystallization of Stage I pyrite and alloclasite to form new minerals, i.e., pure pyrite and chalcopyrite, along with tennantite and siegenite, $(\text{Co}+\text{Ni})_3\text{S}_4$. In general, most of the Stage II sulfide minerals are coarser-grained, and can be identified in hand specimen. However, the siegenite is often intergrown with tennantite/chalcopyrite and, owing to a similarity in atomic mass, can easily be overlooked during SEM-BSE analysis.
- Additional ore minerals identified in this study, in descending order of abundance, include galena, sphalerite, bornite, chalcocite, bismuthinite, and enargite.

- No discrete silver minerals have been observed at Black Butte. Based upon EMPA analyses and assay data, most of the silver is probably contained within the crystal structure of other sulfide minerals, including galena, chalcopyrite and tennantite.
- Along with barite, the Upper Sulfide zone at Black Butte contains appreciable quantities of Ba-rich feldspar, including both hyalophane and celsian (pure $\text{BaAl}_2\text{Si}_2\text{O}_8$). In addition, several zones of apatite-rich ore were found in both the Upper and Lower Sulfide Zones. One LSZ sample rich in apatite also contained abundant siegenite and alloclasite.
- A preliminary examination of C- and O-isotopes in carbonate minerals within the Newland Formation showed no evidence of isotopic anomalies as one approaches the Upper Sulfide Zone from either the footwall or hanging wall of the Black Butte deposit. The isotopic data are consistent with a marine origin for dolomite in the Newland Fm.
- Stage I mineralization was syngenetic and occurred in a classic SEDEX-type of environment by precipitation of fine-grained sulfides out of a dense brine pool. The presence of authigenic carbonates and feldspars suggests a near-neutral pH, while the abundance of sulfide minerals indicates euxinic (H_2S -rich) conditions. However, local deviations to lower pH are required to explain the presence of primary marcasite. These locally-acidic conditions may have been caused by vertical mixing of the overlying water column, resulting in episodic oxidation of H_2S to sulfuric acid.
- Stage II mineralization (which was epigenetic) generated a suite of minerals which provide important temperature and sulfur fugacity constraints for the period. This assemblage, which includes sphalerite, siegenite, and bismuthinite, shows the activity of $\text{S}_2(\text{g})$ ranging from 10^{-21} to 10^{-17} and the temperature ranging from 110°C to 200°C .

There was spatial variation in these conditions, however, as evidenced by the localized presence of minerals indicative of higher aS_2 conditions, such as bornite, chalcocite, and enargite.

- Although the environment of deposition of Black Butte closely resembles that of a classic SEDEX type deposit, the metal associations (i.e., Cu/Co/Ni/Ag as opposed to Pb/Zn) are more similar to those of a red-bed copper deposit. A model is tentatively proposed in which saline brines migrated through the Neihart Quartzite, a laterally extensive, hematite-rich quartz-sandstone located beneath the Newland and Chamberlain Fms., and exhaled onto the sea floor along steeply dipping growth faults.
- Finally, the mineralogical findings of this thesis may have some implications for the milling of the ore. While siegenite typically occurs as individual grains (usually amorphous growth structures) and may be able to be crushed and floated, the cobalt contained within the very fine grained alloclastite and as chemical impurities in pyrite I will likely require more complicated recovery methods (i.e. “roasting”).

5.2. Possible future work

As exploration and development of the Black Butte ore body continues in the near future, there will no doubt be excellent opportunities for continued research. A further investigation of the alloclastite/pyrite spheroids found in Stage I would be interesting, especially if this can be done using EMPA X-ray maps. The electron microprobe was found to have a much higher resolution and sensitivity compared to the SEM, attributes that are critical to resolving the grain size and textural relationships for Co-Ni mineralization in Stage I.

Although sulfur isotope studies have been done at Black Butte, one possible line of investigation would be to perform a S-isotope investigation of the Pb-Zn sulfides on the southern

and western margins of the district, comparing them with Cu-Co-Ni sulfides of the central Johnny Lee and Lowry deposits. Also, now that the paragenesis of the Johnny Lee and Lowry deposits is better constrained, it might be useful to compare the S-isotope systematics of Stage I vs. Stage II sulfide minerals. In addition, it might be instructive to examine C- and O-isotopes of carbonate minerals within the lower Newland Fm. many km away from the zones of high grade Cu mineralization, to see if there is a district-scale zonation in $\delta^{13}\text{C}$ or $\delta^{18}\text{O}$, as has been shown to be the case in Australian SEDEX deposits hosted by dolomitic shale.

Based upon the similarities of the Black Butte mineral suite to that of a red-bed copper deposit, coupled with the proximity of the Neihart Quartzite, it may prove valuable to perform a geochemical investigation of that lithological unit. Possible lines of investigation would include an analysis of the chemistry and crystallinity of iron oxides within the Neihart. It might even be possible to perform some low-temperature leach studies, similar to those of Rose and Bianchi-Mosquera, to see if the Neihart is capable of producing an ore fluid rich in Cu-Co-Ni. Finally, although the contact between the Chamberlain and Neihart Formations has been drilled and found to be lacking visible sulfide mineralization, it may be worthwhile to drill that contact in multiple locales to determine if there is any hint of stratiform copper mineralization similar to a classic red-bed copper deposit.

6. References

- Barton, P. B., & Bethke, M. (1987). Chalcopyrite disease in sphalerite: Pathology and epidemiology. *American Mineralogist*, 72, 451-467.
- Barton, P. B., & Skinner, B. J. (1979). Sulfide mineral stabilities. In H. L. Barnes (Ed.), *Geochemistry of Hydrothermal Ore Deposits* (2nd ed., pp. 278-403). New York: John Wiley and Sons.
- Chandler, F. W. (2000). The Belt-Purcell Basin as a low-latitude passive rift; implications for the geological environment of Sullivan type deposits. In J. W. Lydon, T. Höy, J. F. Slack, & M. Knapp (Ed.), *Geological Environment of the Sullivan Deposit, British Columbia* (Mineral Deposits Division Special Publication 1st ed., pp. 82-112). Geological Association of Canada.
- Childress, J. J., & Fischer, C. R. (1992). The biology of hydrothermal vent animals: Physiology, biochemistry and autotrophic symbioses. *Oceanographic Marine Biology Annual Review*, 30, 337-441.
- Chu, X., Zhang, T., Zhang, Q., & Lyons, T. W. (2007). Sulfur and carbon isotope records from 1700 to 800Ma carbonates of the Jixian section, northern China: Implications for secular isotope variations in Proterozoic seawater and relationships to global supercontinental events. *Geochimica et Cosmochimica Acta*, 71(19), 4668-4692.
- Connor, J. J., Reynolds, M. W., & Whipple, J. W. (1984). Stratigraphy of the Ravalli Group, Belt Basin, Montana and Idaho. In S. W. Hobbs (Ed.), *Special Publication - State of Montana Bureau of Mines and Geology* (Vol. 90, pp. 13-15). Montana Bureau of Mines and Geology.
- Craig, J. R., Vaughan, D. J., & Higgins, J. B. (1979). Phase relations in the Cu-Co-S system and mineral associations of the carrollite (CuCo₂S₄)-linnaeite (Co₃S₄) series. *Economic Geology*, 74, 657-671.
- Degens, E. T., & Ross, D. A. (1969). *Hot Brines and Recent Heavy Metal Deposits in the Red Sea*. New York: Springer-Verlag.
- Drever, J. L. (1997). *The Geochemistry of Natural Waters*. New York: Simon and Schuster.
- Essene, E. J., Claffin, C. L., Giorgetti, G., Mata, P. M., Peacor, D. R., Arkai, P., & Rathmell, M. A. (2005). Two-, three- and four-feldspar assemblages with hyalophane and celsian: implications for phase equilibria in BaAl₂Si₂O₈-CaAl₂Si₂O₈-NaAlSi₃O₈-KAlSi₃O₈. *European Journal of Mineralogy*, 17, Number 4, 515-535.
- Fournier, R. O. (1989). Geochemistry and dynamics of the Yellowstone National Park hydrothermal system. *Annual Reviews in Earth and Planetary Science*, 17, 13-53.
- Godlewski, D. W., & Zieg, G. A. (1984). Stratigraphy and depositional setting of the Precambrian Newland Limestone. *Montana Bureau of Mines and Geology Special Publication*, 90, 2-4.
- Goodfellow, W. D. (2000). Anoxic conditions in the Aldridge Basin during formation of the Sullivan Zn-Pb deposit: Implications for the genesis of massive sulphides and distal hydrothermal sediments. In J. W. Lydon, T. Höy, J. F. Slack, & M. Knapp (Ed.),

- Geological Environment of the Sullivan Deposit, British Columbia* (Mineral Deposits Division Special Publication 1st ed., pp. 12-31). Geological Association of Canada.
- Graham, G., Hitzman, M. W., & Zieg, G. A. (2012). Geologic setting, sedimentary architecture and paragenesis of the sediment-hosted, meso-Proterozoic Black Butte Cu-Co-Ag deposit, Helena Embayment, Montana, USA. *Economic Geology* (in press).
- Grotzinger, J. P. (1986). Shallowing-upward cycles of the Wallace Formation, Belt Supergroup, northwestern Montana and northern Idaho. *Special Publication – State of Montana Bureau of Mines and Geology*, 94, 143-160.
- Gustafson L.B. and Williams N. (1981) Sediment-hosted stratiform deposits of copper, lead, and zinc. In B.J. Skinner, Ed., *Economic Geology 75th Anniversary Volume* (pp. 139-178) Littleton, Colorado: Society of Economic Geologists.
- Himes, M. D., & Petersen, E. U. (1990). Geological and mineralogical characteristics of the Sheep Creek copper-cobalt sediment-hosted stratabound sulfide deposit, Meagher County, Montana. In D. M. Hausen, D. N. Halbe, E. U. Petersen, & W. J. Tafure (Ed.), *Proceedings of the Gold '90 Symposium* (pp. 533-546). Salt Lake City, Utah: Society for Mining, Metallurgy, and Exploration.
- Hitzman, M., Kirkham, R., Broughton, D., Thorson, J., & Selley, D. (2005). The sediment-hosted stratiform copper ore system. In J. W. Hedenquist, J. F. Thompson, R. J. Goldfarb, & J. P. Richards (Eds.), *Economic Geology 100th Anniversary Volume* (pp. 609-642). Littleton, Colorado: Society of Economic Geologists.
- Holland, H. D., & Malinen, S. D. (1979). The solubility and occurrence of non-ore minerals. In H. L. Barnes (Ed.), *The Geochemistry of Hydrothermal Ore Deposits* (2nd ed., pp. 461-508). Wiley.
- Höy, T., Anderson, D., Turner, R. J., & Leitch, C. H. (2000). Tectonic, magmatic, and metallogenic history of the early synrift phase of the Purcell Basin, southeastern British Columbia. In J. W. Lydon, T. Höy, J. F. Slack, & M. Knapp (Ed.), *Geological Environment of the Sullivan Deposit, British Columbia* (Mineral Deposits Division Special Publication 1st ed., pp. 32-60). Geological Association of Canada.
- Keefer, W. R. (1972). Geologic map of the west half of the Neihart 15-minute quadrangle, central Montana. *U.S. Geol. Surv. Misc. Geol. Invest. Map I-726*.
- Large, R. R., Bull, S. W., & Winefield, P. R. (2001). Carbon and oxygen isotope halo in carbonates related to the McArthur River (HYC) Zn-Pb-Ag deposit, North Australia: Implications for sedimentation, ore genesis, and mineral exploration. *Economic Geology*, 96, number 7, 1567-1593.
- Le Bris, N., Sarradin, P., & Caprais, J. (2003). Contrasted sulphide chemistries in the environment of 13 degrees N EPR vent fauna. *Deep-Sea Research I*, 50, 737-747.
- Leach, D. L., Sangster, D. F., Kelly, K. D., Large, R. R., Garven, G., Allen, C. R., . . . S, W. (2005). Sediment-hosted lead-zinc deposits: A global perspective. In J. W. Hedenquist, J. F. Thompson, R. J. Goldfarb, & J. P. Richards (Eds.), *Economic Geology 100th Anniversary Volume* (pp. 561-607). Littleton, Colorado: Society of Economic Geologists.

- Lydon, J. W. (2007). Geology and metallogeny of the Belt-Purcell Basin. In W. D. Goodfellow (Ed.), *Mineral Deposits of Canada: A Synthesis of Major Deposit-Types, District Metallogeny, the Evolution of Geological Provinces, and Exploration Methods. Geological Association of Canada, Mineral Deposits Division, Special Publication No. 5*, p. 581-607.
- Lyons, T. W., Luepke, J. J., Schreiber, M. E., & Zieg, G. A. (2000). Sulfur geochemical constraints on Mesoproterozoic restricted marine deposition; lower Belt Supergroup, Northwestern United States. *Geochimica et Cosmochimica Acta*, *64*, 427-437.
- Maxwell, D. T., & Hower, J. (1967). High grade diagenesis and low grade metamorphism of illite in the Precambrian Belt Series. *American Mineralogist*, *52*, 843-857.
- McGoldrick, P., & Zeig, G. A. (2004). Massive microbes from the Mesoproterozoic of Montana. *Australian Geological Convention*. Hobart, Australia. Abstract of Oral Presentation.
- McMannis, W. J. (1963). LaHood Formation; A coarse facies of the Belt Series in southwestern Montana. *Geological Society of America Bulletin*, *74*, 407-436.
- Murowchick, J. B. (1984). The formation and growth of pyrite, marcasite, and cubic FeS:. Unpublished PhD Dissertation, Pennsylvania State University, 168p.
- Murowchick, J. B. (1992). Marcasite inversion and the petrographic determination of pyrite ancestry. *Economic Geology*, *87*, 1141-1152.
- Nelson, W. H. (1963). *Geology of the Duck Creek Pass quadrangle, Montana*. US Geological Survey, Bulletin 1121J, 56 pp.
- Nesse, W. D. (2012). *Introduction to Optical Mineralogy*. USA: Oxford University Press.
- Petersen, E. U. (1989). *Mineralogical and Compositional Study of Sheep Creek Ores*. BHP-Utah International Inc. Report 6-1 BMH.R, June, 63p.
- Price, R. (1964). The Precambrian Purcell System in the Rocky Mountains of southern Alberta and British Columbia. *Bulletin of Canadian Petroleum Geology*, *12*, pp. 399-426.
- Price, R. A., & Sears, J. W. (2000). A preliminary palinspastic map of the Mesoproterozoic Belt-Purcell Supergroup, Canada and USA; implications for the tectonic setting and structural evolution of the Purcell Anticlinorium and the Sullivan Deposit, British Columbia. In J. W. Lydon, T. Höy, J. F. Slack, & M. Knapp (Ed.), *Geological Environment of the Sullivan Deposit, British Columbia* (Mineral Deposits Division Special Publication 1st ed., pp. 61-81). Geological Association of Canada.
- Ray, J. S., Veizer, J., & Davis, W. J. (2003). C, O, Sr and Pb isotope systematics of carbonate sequences of the Vindhyan Supergroup, India: age, diagenesis, correlations, and implications for global events. *Precambrian Research*, *121*, 103-140.
- Richardson, F. D., & Jeffes, J. H. (1952). The thermodynamics of substances of interest in iron and steel making. III. Sulfides. *J. Iron Steel Inst.*, *171*, 165-175.
- Rose, A. W., & Bianchi-Mosquera, G. C. (1993). Adsorption of Cu, Pb, Zn, Co, Ni, and Ag on goethite and hematite: A control on metal mobilization from red beds into stratiform copper deposits. *Economic Geology*, *88*, 1226-1236.

- Ross, G. M., & Villeneuve, M. (2003). Provenance of the Mesoproterozoic (1.45 Ga) Belt Basin (western North America): Another piece in the pre-Rodinia paleogeographic puzzle. *Geological Society of America Bulletin*, 115, 1191-1217.
- Schieber, J. (1985). The relationship between basin evolution and genesis of stratiform sulfide horizons in Mid-Proterozoic sediments of Central Montana (Belt Supergroup). Unpublished PhD Thesis, University of Oregon, 811pp.
- Schieber, J. (1989). Facies and origin of shales from the Mid-Proterozoic Newland Formation, Belt Basin, Montana, U.S.A. *Sedimentology*(36), 203-219.
- Schieber, J. (1991). The origin and economic potential of disseminated Pb-Zn mineralization in pyritic shale horizons of the Mid-Proterozoic Newland Formation, Montana, U.S.A. *Mineralium Deposita*, 26, 290-297.
- Schieber, J. (2007). Microbial mat features in terrigenous clastics of the Belt Supergroup, Mid-Proterozoic of Montana, USA. In J. Schieber, P. K. Bose, P. G. Eriksson, S. Banarjee, S. Sarkar, W. Altermann, & O. Catuneau (Ed.), *Atlas of Microbial Mat Features Preserved Within the Clastic Rock Record* (pp. 158-170). Elsevier.
- Scott, S. D., & Barnes, H. L. (1971). Sphalerite geothermometry and geobarometry. *Economic Geology*, 66, 653-669.
- Sears, J.W. (2007) Belt-Purcell Basin: Keystone of the Rocky Mountain fold-and-thrust belt, United States and Canada. *Geological Society of America, Special Paper 433*, 147-166.
- U.S. Geological Survey. (2009). U.S Geological Survey Data Series 140. In T. D. Kelly, & G. R. Matos, *Historical statistics for mineral and material commodities in the United States*. Retrieved December 2011, from <http://pubs.usgs.gov/ds/2005/140/>
- Weed, W. H. (1900). Geology of the Little Belt Mountains: *U.S. Geological Survey 20th Annual Report, pt 3*.
- Winston, D. (1986a). Middle Proterozoic tectonics of the Belt Basin, western Montana and northern Idaho. In Roberts, S.M. ed., Belt Supergroup. *Montana Bureau of Mines and Geology, Special Paper 94* 245-257.
- Winston, D. (1986b) Stratigraphic correlation and nomenclature of the Middle Proterozoic Belt Supergroup, Montana, Idaho, and Washington. In Roberts, S.M. ed., Belt Supergroup. *Montana Bureau of Mines and Geology, Special Paper 94*, 69-84.
- Woodward, L. A. (1983). Structural geology of the Helena Salient: A synopsis: Guidebook of the thrust and fold belt, west central Montana. In Smith, D. L. ed. *Montana Bureau of Mines and Geology, Special Publication*, 86, 83-88.
- Yang, H., & Downs, R. T. (2008). Crystal structure of glaucodot, (Co,Fe)AsS, and its relationships to marcasite and arsenopyrite. *American Mineralogist*, 93, 1183-1186.
- Zieg, G. A. (1986). Stratigraphy and sedimentology of the Middle Proterozoic upper Newland Limestone. In S. M. Roberts (Ed.), Belt Supergroup. *Montana Bureau of Mines and Geology, Special Publication*, 94, 125-141.

- Zieg, G. A., & Leitch, C. H. (1998). The geology of the Sheep Creek copper deposits, Meagher County, Montana. In *Belt Symposium III (Comp. R. Berg) Abstracts Montana Bureau of Mines and Geology Open File Report* (Vol. MBMG 381).
- Zieg, G. A., Rankin, P. W., Hall, S. M., & Tureck-Schwartz, K. R. (1991). The geology of the Sheep Creek Proterozoic copper deposits, central Montana. *Society of Mining Engineers of AIME preprint, Rocky Mountain Section*. Denver.

Appendix A: Photomicrograph Locations

Photomicrograph	Hole	Depth (m)	Sulfide Zone	Photomicrograph	Hole	Depth (m)	Sulfide Zone
Plate 1				Plate 6			
A	SC11-016	56.1	USZ	A	SC10-006	275.8	LSZ
B	SC11-024	176.8	USZ	B	SC10-006	275.8	LSZ
C	SC11-016	70.0	USZ	C	SC10-006	275.8	LSZ
D	SC11-026	154.0	USZ	D	SC10-006	275.8	LSZ
E	SC11-006	416.4	LSZ	E	SC10-005	411.8	LSZ
F	SC11-031	103.2	USZ	F	SC10-005	411.8	LSZ
Plate 2				Plate 7			
A	SC10-005	411.8	LSZ	A	SC11-018	73.5	USZ
B	SC10-005	411.8	LSZ	B	SC11-018	73.5	USZ
C	SC11-031	89.4	USZ	C	SC11-018	73.5	USZ
D	SC11-018	73.5	USZ	D	SC11-018	73.5	USZ
E	SC11-027	35.9	USZ	E	SC11-029	66.8	USZ
F	SC11-024	193.2	USZ	F	SC11-029	66.8	USZ
Plate 3				Plate 8			
A	SC11-024	170.7	USZ	A	SC11-029	64.3	USZ
B	SC11-021	129.2	USZ	B	SC11-029	68.8	USZ
C	SC11-029	71.6	USZ	C	SC11-029	64.3	USZ
D	SC11-031	67.2	USZ	D	SC11-029	64.3	USZ
E	SC10-006	274.8	LSZ	E	SC11-029	68.8	USZ
F	SC10-006	274.8	LSZ	F	SC11-018	73.5	USZ
Plate 4				Plate 9			
A	SC11-029	71.6	USZ	A	SC11-029	64.3	USZ
B	SC11-021	139.1	USZ	B	SC11-029	64.3	USZ
C	SC11-027	83.5	USZ	C	SC11-024	170.7	USZ
D	SC11-021	139.1	USZ	D	SC10-006	416.4	LSZ
E	SC11-018	75.0	USZ	E	SC11-016	70.1	USZ
F	SC11-029	72.6	USZ	F	SC11-016	70.1	USZ
Plate 5							
A	SC10-005	411.8	LSZ				
B	SC10-005	411.8	LSZ				
C	SC10-005	411.8	LSZ				
D	SC10-005	411.8	LSZ				
E	SC10-005	411.8	LSZ				
F	SC10-005	411.8	LSZ				

Appendix B: EDS Analyses

(Analyses performed with SEM located at the CAMP at Montana Tech)

Siegenite

Analysis	S	Fe	Co	Ni	Cu
	weight percent				
1	41.22	4.37	22.88	31.52	0
2	40.8	0	22.05	30.97	6.18
3	39.84	0.85	21.52	31.79	6
4	41.77	6.32	23.01	28.9	0
5	40.88	0	20.8	33.85	4.47
6	40.09	8.29	19.44	26.79	5.39
7	40.88	0	20.85	33.66	4.6
8	38.49	0.95	29.97	21.1	9.49
9	38.72	0.83	29.97	18.96	11.53
10	38.73	0.99	30.33	19.83	10.11
11	30.43	1.57	30.49	19.64	9.87
	atomic percent				
1	56.16	3.42	16.96	23.46	0
2	56.02	0	16.47	23.22	4.28
3	55.01	0.67	16.17	23.97	4.18
4	56.68	4.92	16.98	21.42	0
5	56.05	0	15.52	25.34	3.09
6	55.08	6.54	14.53	20.11	3.74
7	56.05	0	15.55	25.21	3.19
8	53.72	0.76	22.76	16.08	6.68
9	54.02	0.66	22.75	14.45	8.12
10	53.99	0.79	23	15.1	7.11
11	53.65	1.26	23.16	14.98	6.96

Pyrite I

Analysis	S	Fe	Co	Ni	As	O	Al	Si	Cu	Zn
	weight percent									
1	34.05	27.09	7.29	5.36	16.01	6.7	1.41	2.1	0	0
2	48.32	42.33	2.87	0.9	5.57	0	0	0	0	0
3	53.39	44.31	0	2.3	0	0	0	0	0	0
4	52.2	45.5	0	2.01	0	0	0	0	0.29	0
5	50.91	46.15	0	2.93	0	0	0	0	0	0
6	47.42	37.21	7.51	4.38	0	0	0	0	3.49	0
7	48.95	41.88	0	0	0	0	0	0	9.17	0
8	50.57	44.9	0	0	0	0	0	0	4.52	0
9	51.3	46.28	0	0	0	0	0	0	0.55	1.87
10	47.2	10.26	0	0	0	0	0	0	12.54	0
	atomic percent									
1	42.11	19.24	4.91	3.62	8.47	16.61	2.07	2.97	0	0
2	62.7	31.54	2.03	0.64	3.1	0	0	0	0	0
3	66.66	31.76	0	1.57	0	0	0	0	0	0
4	65.6	32.84	0	1.38	0	0	0	0	0.18	0
5	64.44	33.54	0	2.03	0	0	0	0	0	0
6	61.57	27.74	5.3	3.11	0	0	0	0	2.28	0
7	63.06	30.98	0	0	0	0	0	0	5.96	0
8	64.31	32.79	0	0	0	0	0	0	2.9	0
9	64.88	33.6	0	0	0	0	0	0	0.35	1.16
10	61.58	30.16	0	0	0	0	0	0	8.26	0

Ba-Feldspar

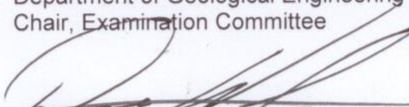
analysis	O	Al	Si	K	Ba	S	Fe
	weight percent						
1	29.09	13.52	32.69	10.88	13.81	0	0
2	28.7	13.22	33.47	11.65	12.96	0	0
3	30.18	15.08	16.93	0	35.56	1.18	1.06
4	28.33	13.87	34.55	14.97	8.28	0	0
5	29.76	13.31	35.99	15.78	5.16	0	0
6	27.33	13.66	36.1	13.3	9.17	0.44	0
7	25.84	14.21	31.36	10.13	18.46	0	0
8	29.45	12.43	38.15	16.69	3.28	0	0
	atomic percent						
1	47.08	12.97	30.14	7.21	2.6	0	0
2	46.38	12.66	30.81	7.71	2.44	0	0
3	56.1	16.62	17.93	0	7.7	1.09	0.56
4	44.73	12.99	31.08	9.68	1.52	0	0
5	45.63	12.11	31.44	9.9	0.92	0	0
6	43.57	12.91	32.78	8.68	1.7	0.35	0
7	44.23	14.42	30.57	7.09	3.68	0	0
8	44.78	11.21	33.04	10.39	0.58	0	0

SIGNATURE PAGE

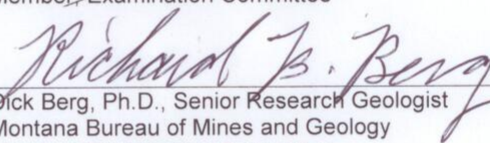
This is to certify that the thesis prepared by Joshua White entitled "Paragenesis of Cobalt and Nickel at the Black Butte Copper Project, Meagher County Montana" has been examined and approved for acceptance by the Department of Geological Engineering, Montana Tech of The University of Montana, on this 10th day of May, 2012.



Christopher Gammons, Ph.D., Professor
Department of Geological Engineering
Chair, Examination Committee



Diane Wolfgram, Ph.D., Professor
Department of Geological Engineering
Member, Examination Committee



Dick Berg, Ph.D., Senior Research Geologist
Montana Bureau of Mines and Geology
Member, Examination Committee